Carbon content driven high temperature γ-α2 interface modifications and stability in Ti–46Al–4Nb intermetallic alloy

Manuscript Details

Manuscript number	INTERMETALLICS_2019_1018_R1
Title	Carbon content driven high temperature gamma-alpha2 interface modifications and stability in Ti-46Al-4Nb intermetallic alloy
Article type	Research paper

Abstract

The effect of carbon addition on the microstructure modifications and hardness response of a two-phase lamellar Ti-46Al-4Nb intermetallic alloy was studied. The alloy was heat treated as to have an initial two-phase refined lamellar microstructure consisitng of alpha2 laths and gamma phase characterized by nanometric wide twinning. The effect of carbon in solid solution in the alpha2 phase and the onset of the H-Ti2AlC phase precipitation within the gamma phase was addressed. A threshold carbon limit of C = 3000 wt. ppm was identified as lower limit solute concentration for the precipitation of the H phase particles. The major alloy hardening factors were identified as the refined interlamellar spacing, the fine twinning and the amount of carbon in solid solution. The role of H phase formation on the alloy hardening with carbon content was addressed and it was essentially such to induce a hardening saturation effect.

Keywords	TiAl intermetallic alloy; interstitial elements; gamma-lamellae interface; twinning; transmission electron microscopy; microhardness.

Corresponding Author	Marcello Cabibbo
Order of Authors	Marcello Cabibbo

Suggested reviewers	Sergey Zherebtsov, Zuzanka Trojanova, Maurizio Vedani, Filip Pruša, Dmytro Orlov

Submission Files Included in this PDF

File Name [File Type]

cover letter.docx [Cover Letter]

Reply letter for Intermetallics 2019_1018.docx [Response to Reviewers]

man Ti46Al4Nb text-only (marked Revised).docx [Revised Manuscript with Changes Marked]

Highlights.docx [Highlights]

graphical Abs.tif [Graphical Abstract]

man Ti46Al4Nb.docx [Manuscript File]

Fig 1a.jpg [Figure]

Fig 1b.tif [Figure]

Fig 2a.tif [Figure]

Fig 2b.tif [Figure]

Fig 3.tif [Figure]

Fig 4.tif [Figure]

Fig 5a.tif [Figure]

Fig 5b.tif [Figure]

Fig 5c.tif [Figure]

Fig 5d.tif [Figure]

Fig 6.tif [Figure]

Fig 7a.tif [Figure]

Fig 7b.tif [Figure]

Fig 7c.tif [Figure]

Fig 7d.tif [Figure]

Fig 7e.tif [Figure]

Fig 8.tif [Figure]

Fig 9.tif [Figure]

conflict of interest statement.pdf [Conflict of Interest]

Author Statement.docx [Author Statement]

Data in brief.docx [Data in Brief]

To view all the submission files, including those not included in the PDF, click on the manuscript title on your EVISE Homepage, then click 'Download zip file'.

Cover letter

The present manuscript entitled: “Carbon content driven high temperature γ-α_2 interface modifications and stability in Ti-46Al-4Nb intermetallic alloy” by Marcello Cabibbo (DIISM / Università Politecnica delle Marche, Via Brecce Bianche 12, 60131 – Ancona, Italy) focuses on the role of different amount of carbon addition on the lamellae morphology and twining character in a two-phase ternary Ti-46Al-4Nb intermetallic alloy. The material, objectives and methodologies of the manuscript are within the aims and scopes of the journal. The study presented in the present manuscript can be considered a new scientific contribution of similar other studies already published in the *Intermetallics* journal.

Yours, sincerely,
Prof. Marcello Cabibbo

Reply letter to Reviewers

Man number Intermetallics_2019_1018

I wish to express my acknowledgement for the useful, constructing and positive comments of all the three Reviewers that have dedicate some time to carefully read and comment on this work.
Hereafter all three Reviewers comments and remarks are addressed point-by-point.

Rev. #1
(1). The relationship between microstructure formation and the content of carbon should be discussed more systematically.
Paragraph 3.2 now reads" Influence of carbon content on the alloy microstructure" and all the details and result reports on the influence of the heat treatment on the Ti-46Al-4Nb microstructure was moved to the end of the previous Par. 3.1 (Microstructure modifications induced by the aging treatments (Ti-46Al-4Nb alloy)).

(2). Hall–Petch (HP) mechanism is generally suited to the microstructure with micrometer scale, however, the microstructure size in this study are in the nano-scale region, the author should explain the applicability of Hall–Petch mechanism in this study.
The following was added at the end of the Paragraph 3.3. Correlation between hardness and microstructure: "As for the validation of the HP relationship reported in Eqs. 1(a)-to-(c), a number of previously published papers accounted on a similar relationship between hardness and lamellar Ti-Al alloy interface spacing [**60,62-64**]. Thus, according to the HP mechanism, interfaces, such as the γ/α_2 and the γ/γ, act as obstacles for the glide of dislocations. Therefore, the HP can still be expressed in the form of the here reported Eqs. 1 (a)-to-(c), since the alloy structure is formed by conventional coarser grains (being in the submicrometer scale well above ~500 nm). That is, an Orowan-type dislocation behavior is acting in the alloy, where dislocations are confined to individual lamellae, which are responsible for a general trend of hardness rise as the lamellar spacing is refined. The hardness increment can be effectively described by HP relationship as shown here. With this respect, Dehm *et al.* [**60**] reported quite a similar phenomenon in a complex Ti-Al based alloy with average interface spacings of ~100 nm. They found that dislocation motion within the γ-phase determines the alloy mechanical properties including hardness, described by a classical HP relationship and taking into consideration the dislocation obstacles constitttuted by the lamellae boundaries."

(3). The study about the relationship between the carbon addition and the interface spacing as well as the lamellae widths is noverty, however, I think it could be expressed more succinctly.
The role of carbon addition to the microstructure modification and, namely, to the interface spacing is one of the two main experimental findings in this work. Thence, I believe that the description and discussion appearing in the Results and discussion section about this novel finding deserves to have the length in the manuscript of that of the present form. I hope to find the Reviewer's understanding about this issue.

Rev. #2
All the following issues, comments and suggestions were addressed in the manuscript and these are marked in yellow in the revised marked word document now appended.
<u>Abstract</u>: Fifth row from the bottom – the simplified phrase „...precipitation of the H phase particles" suits better.
Done.

<u>Introduction</u>:
Secon paragraph – fifth row is missing a hyphen (The α2-Ti....)
Third paragraph: the phase transformation sequences shall preferably contain arrows instead of dashes (or plus signs in the experimental section).

The author is mentioning, that the addition of C, O, N and its influence of the Ti-Al alloys has been already studied and published in several publications which shall be accompanied by proper bibliographic citations.
Done.

Experimental:
The author shall describe in more detail the powder metallurgy technique used for the preparation of alloys. The author shall also provide information about the chemical analysis regarding especially the determination of the C content within the alloy.
The following was added in the Experimental details section:
"The alloys were prepared by powder metallurgy (PM) to obtain a homogeneous chemical distribution of the substitutional elements (Al, Nb). Ti, Al, Nb, and eventually C, were mixed together for 2 h by using a ball mill process in a dedicated chamber saturated with argon atmosphere. The rotational speed was fixed to 180 rounds per minute with a mass-to-ball ratio of 3:1. The mixture was then uniaxially compacted by hot isostatic pressing (HIP) at 1573K at a pressure of 170 MPa for 6 h, and then cooled at a rate of 20K/min ,reaching a compacted alloy with a density of 3.95 g/cm^3. In the carbon-bearing alloys, the carbon wt. content was measured by electronic balance using a Radwag™ AS82-220.R2® analytical balance."

Results, discussion, conclusion:
The author mentioned in Table 1 that the lowest content of C has been chosen as 500 ppm, thus I believe, that the value of 300 ppm in the second row shall be corrected.
Correct, this had to read 500 ppm and it was corrected.

The Burges vector of the dislocations loop shall be checked since there is a sharp bracket instead of a square bracket.
Done.

Section 3.2. – second paragraph – the author is mentioning table 1 regarding the width of the γ lath (which are not mentioned there).
This quotation was deleted as in the Table there were not data referring to the γ-lath width.

Please, check words like: bedue, grained boundary density, Corresppndingly, etc.. Also, some of the cross-links are missing (e.g. for Table 3 etc.).
Done throughout the text body.

Rev. #3
1. Heat treatment in a graphical form would be more apprehensible for the readers (rather than a table form).
A scheme of the heat treatment to which the alloys were subjected is now reported in the new Fig. 1 a and reference to it was added in the text body.

2. How the "interface reaction" drives the "occurrence of the observed lamellar spacing widening"?
The following sentences were added in the text body:
"Thus, interface reactions between the thin lamellar plates are promoted and driven by the aging temperature. This, in turns, drives the occurrence of the observed lamellar spacing widening. That is, some of the existing interfaces, during second aging treatment are induced to react each other. Thence, thin lamellar plates take place during aging to eventually coarsening the lamellar spacing."

3. It seems that some references to Tables are confused. For example, are references on Table 1 in section 3.2 correct? And there is no any reference on Table 3 in the text.
Thank you for this remark. References to the manuscript Tables were checked and corrected where needed. In particular, the here mentioned quotation now reads:

“The width of the α_2 laths decreased by rising the second annealing temperature, as shown by the experimental data reported in **Figure 3**.”
And in the following:
“In this case, the α_2 lath width slightly widened to remain constant with further C addition to the Ti-46Al-4Nb alloy up to 0.5 wt.% (**Table 3**).”

4. It is not quite clear if carbon decrease or increase the stacking-fault energy? Literature gives quite controversial data.
Yes, this is somehow true. With this respect, since the present work did not deal specifically on the relationship and calculation of SFE and carbon content in the Ti-46Al-4Nb alloy, the following was added in the manuscript section 3.2. “Influence of carbon content on the alloy microstructure”:
“In addition, the self diffusion of carbon within the γ-phase is chiefly driven by its diffusion activation energy that is considerably lower than that of niobium. It was also observed that as the carbon content in the alloy rises, the occurrence of perfect-twins (Pe-T) within the alloy microstructure increases significantly. Indeed, the change in the interface character is associated with the difference in interfacial energy among the three types of twin interfaces. In turns, the interfacial energy for each type of twinning can roughly be evaluated by bond energy of atom pair across the interface itslef. On this basis, even if in the present study no calculations were made to determine the alloy stacking fault energy (SFE), it is believed that the increment of Pe-T at the expense of the other partial twins, such as the variant-twins (V-T) and the pseudo-twins (Ps-T), is likely to induce a SFE redcution. This is likely to be the case until carbon does not saturate and the precipitation of a *H*-Ti_2AlC phase occur at the expense of the carbon in solid solution within the γ-grain. Infact, starting from a carbon content above 3000 wt. ppm, the precipitation of the *H*-Ti_2AlC phase occurred progressively draining all the carbon in solid solution within the γ-phase. This, in turns, is likely to further reduce the alloy SFE as the Pe-T recorded a consistent increment at the expense of the Ps-T and the V-T. Yet, to properly address this somehow important issue, further insights are needed. These will have to be using specific and systematic approaches to determine the actual relationship between the different carbon concentration in the C-bearing lamellar Ti-46Al-4Nb alloys and their resulting SFE.”

Dear Editor, dear Reviewers, I strongly hope to have exhaustively and effectively addressed all the comments and remarks made to improve and make this manuscript suitable for publication in *Intermetallics* journal.

Yours,
Sincerely.

Prof. Marcello Cabibbo

Carbon content driven high temperature γ-α_2 interface modifications and stability in Ti-46Al-4Nb intermetallic alloy

Marcello Cabibbo

DIISM / Università Politecnica delle Marche, Via Brecce Bianche 12, 60131-Ancona, Italy.

Abstract.

The effect of carbon addition on the microstructure modifications and hardness response of a two-phase lamellar Ti-46Al-4Nb intermetallic alloy was studied. The alloy was heat treated as to have an initial two-phase refined lamellar microstructure consisitng of α_2 laths and γ phase characterized by nanometric wide twinning. The effect of carbon in solid solution in the α_2 phase and the onset of the H-Ti_2AlC phase precipitation within the γ phase was addressed. A threshold carbon limit of C ≅ 3000 wt. ppm was identified as lower limit solute concentration for the precipitation of the H phase particles. The major alloy hardening factors were identified as the refined interlamellar spacing, the fine twinning and the amount of carbon in solid solution. The role of H phase formation on the alloy hardening with carbon content was addressed and it was essentially such to induce a hardening saturation effect.

Keywords: TiAl intermetallic alloy; interstitial elements; γ-lamellae interface; twinning; transmission electron microscopy.

1. Introduction

Owing to their high specific strength, low density and good oxidation resistance, the class of γ-titanium aluminides are very interesting materials for structural use at elevated temperatures [**1,2**]. These alloys have excellent properties compared to other high-temperature resistant metallic materials, such as Ni- and Co-based superalloys. In particular, two phase γ-TiAl based alloys with a fully lamellar structure have attracted significant interest due to their outstanding creep resistance and fracture toughness [**3-6]**

The typical microstructure of this class of alloys consists of alternating α_2-lamellae and γ-plates, which are formed during cooling from the parent α phase. The mutual crystallographic relationship is as (0001)-α_2 || (111)-γ and <1120>-α_2 || <110>-γ [**3**]. The γ-TiAl has a $L1_0$ face-centred tetragonal (FCT) crystal structure with lattice parameters a = 0.4005 nm and c = 0.4070 nm. The primary deformation modes of the γ phase are <110> slip and {111}<112> twinning [**7**]. The α_2-Ti_3Al phase has a DO_{19} hexagonal close-packed (HCP) crystal structure with lattice parameters a = 0.579 nm and c = 0.467 nm. Ti_3Al preferentially deforms in the prismatic {10-10}1/6<11-20> slip directions, the basal {0001}1/6<11-20> directions, and the pyramidal {10-2-1}1/6<11-26> directions [**8**].

This duplex microstructure improves the alloy ductility, while, the lamellar structure promotes fracture toughness and creep resistance [**9**]. In particular, a number of factors influence the lamellar structure and the resulting alloy mechanical properties [**10**]. These are the α_2 volume fraction, $F_V(\alpha_2)$, the α_2 lamellae width, $\lambda_{\alpha 2}$, and the lamellae spacing, S_l. It is well known that the lamellae spacing is a dominant factor influencing the alloy hardness, as this increases by reducing the lamellae spacing [**11**]. With this regards, Schillinger *et al.* [**12**] showed that ultrafine lamellae improve the short-term creep behavior of Ti–46Al-1.5Cr–2Mo–X alloys. Thus, different heat treatments and alloying

element addition were used as a strategy to drive and control the lamellae spacing in fully lamellar structured γ-TiAl based alloys [**11,13-16**]. Recently, using multistep heat treatments, Clemens *et al.* [**17**] reported on successfully refined fully lamellar structures in different γ-TiAl based alloys. Usually, lamellar structures can form by one of the following two kinds transformation sequence induced by heat treatment: $\alpha \rightarrow (\alpha+\gamma) \rightarrow (\alpha_2+\gamma)$, or $\alpha \rightarrow \alpha_2 \rightarrow (\alpha_2+\gamma)$ [**18**]. These two reactions actually correspond to a different lamellar structure, as in the first case the alloy is characterized by a conventional lamellar structure, that is, lamellae with usual width, $\lambda_{\alpha 2}$. On the contrary, in the second case, ultrafine lamellar structures are induced to form.

For usual lamellar microstructures different researchers studied the role of heat treatment, alloying elements and other microstructure features on the lamellae formation mechanisms in γ-Ti-Al based alloys [**13,19-27**]. Other research works addressed the microstructure and mechanical characterization of ultrafine lamellar structure Ti-Al based alloys [**15,16,18**]. It resulted that understanding the factors affecting the lamellae width, $\lambda_{\alpha 2}$ and their thermal stability, both in terms of alloying elements (Nb being one of the most important element in such alloys) and in terms of specific heat treatments is a key issue in Ti-Al based intermetallic alloys. Among the different usually added elements, carbon and the other interstitial elements, along with heat treatments, is known to significantly modify both lamellae width $\lambda_{\alpha 2}$, and spacing, S_l, and their thermal stability and character. With this regard, studies on the effects of all interstitial elements, such O, N, C, on the microstructure modifications and the mechanical properties of the Ti-Al alloys were published in several contributions. In particular, in the TiAl γ phase the solubility of O, N or C is low, and then precipitate particles tend to form by both prolonged heat treatments and interstitial content **[28-33]**. On the other hand, the interstitial elements have high solubility within the hexagonal α_2 phase. Thus, strong interactions among the existing interstitital elements within the matrix, the sliding dislocations induced during plastic deformation, and the existing particles characterize the mechanical response of such interstitial-bearing alloys **[34].**

Upon high temperature and cooling treatment sequences of Ti-Al lamellar-structured alloys, lamellae interfaces are not only of the type α_2/γ but also many γ/γ interfaces are also present. This results from alloy cooling, by wich the fraction of γ plates is induced to rise up to values for which γ interfaces start to meet. Moreover, γ/γ interfaces can be crystallographically classified into three different types; variant interface twin (V-T), pseudo-twin (Ps-T), and perfect-twin (Pe-T) boundaries [**2,9,10**]. Thus, the alloy thermal stability is likely to chiefly depends on the stability and character of both the α_2/γ and the γ/γ interfaces.

The addition of a ternary element to the Ti-Al alloy, such as Cr, Mn, V, and Nb is considered necessary to improve the room-temperature ductility and fracture toughness of the two-phase Ti-Al intermetallic alloys [**34-37**]. Both mechanical properties are usuually improved by microstructural induced modifications and by slip and twin deformation driven by the solute elements [**38-43**]. In particular, the addition of Nb makes the α to γ transformation kinetics sluggish **[43,44]**. By a microstructure viewpoint Nb addition in the two phase Al-Ti alloys distributes equally into α and γ phases. Thence, no segregation of Nb takes place at the lamellae interface boundaries. That is, the Nb addition in the alloy does not influence the stability among the different lamellae interfaces [**44**].

Following the here reported state of the art, this study focuses on the role of different amount of carbon addition on the lamellae morphology and twining character in a two-phase ternary Ti-46Al-4Nb intermetallic alloy. In particular, the influence of the heat treatment, namely two aging temperatures, was addressed to determine the lamellae stability and the twin interface character in the Ti-Al-Nb added with increasing amount of carbon, from a minimum of (wt.%) C = 500 ppm, to a maximum of 5000 ppm (C=0.5%).

2. Experimental details

In this study an Ti-46Al-4Nb (Ti-46-4) alloy added with different amount of carbon was used. **Table 1** reports the alloy chemical composition, the exact amounts of the interstitial element (C) added to the alloy, and the two different thermal treatments to which all the C-modified Ti-46-4 intermetallic alloys were subjected.

The alloys were prepared by powder metallurgy (PM) to obtain a homogeneous chemical distribution of the substitutional elements (Al, Nb). Ti, Al, Nb, and eventually C, were mixed together for 2 h by using a ball mill process in a dedicated chamber saturated with argon atmosphere. The rotational speed was fixed to 180 rounds per minute with a mass-to-ball ratio of 3:1. The mixture was then uniaxially compacted by hot isostatic pressing (HIP) at 1573K at a pressure of 170 MPa for 6 h, and then cooled at a rate of 20K/min ,reaching a compacted alloy with a density of 3.95 g/cm^3. In the carbon-bearing alloys, the carbon wt. content was measured by electronic balance using a Radwag™ AS82-220.R2® analytical balance.

Lamellar microstructure was obtained by rapidly cooling the single-phase hexagonal α phase alloy from 1573K through the temperature range of 1523 to 1473K [**45**]. Ultrafine lamellar microstructure consisting of $\gamma + \alpha_2$ phases was obtained by a two-step heat treatment. The first step of the heat treatment consisted of heating above the $T_{\alpha\text{-transus}}$ temperature (1423K/1h) [**46**], followed by oil quenching (OQ) to room temperature (RT) at a cooling rate sufficiently rapid to suppress the α to $\alpha + \gamma$ to $\alpha_2 + \gamma$ transformation. That is, a direct α to α_2 transformation was induced. The second step consisted on heating the alloys to 1173 or 1273K at a rate of 25K/min, immediately followed by OQ. **Figure 1 (a)** reports a schematic representation of the here described heat treatments. This two-step heat treatment was able to induced the formation of an ultrafine lamellar structure.

	Ti-46-4	Ti-46-4-C$_1$	Ti-46-4-C$_2$	Ti-46-4-C$_3$	Ti-46-4-C$_4$	Ti-46-4-C$_6$
Chemical composition, wt.%	46Al, 4Nb	46Al, 4Nb, C(500ppm)	46Al, 4Nb, C(1000ppm)	46Al, 4Nb, C(2000ppm)	46Al, 4Nb, C(3000ppm)	46Al, 4Nb, C(5000ppm)
2nd heating T, K/h	T$_1$=1173/1 cooling 15K/min T$_2$=1273/1 cooling 25K/min	T$_1$=1173/1 cooling 15K/min T$_2$=1273/1 cooling 25K/min	T$_2$=1273/1 cooling 25K/min	T$_2$=1273/1 cooling 25K/min	T$_2$=1273/1 cooling 25K/min	T$_2$=1273/1 cooling 25K/min
Hardness, HV$_5$	T$_1$:410±10 T$_2$:440±10	T$_1$:420±10 T$_2$:440±10	T$_2$:490±10	T$_2$:515±5	T$_2$:540±10	T$_2$:545±5
F$_V$(α_2), %	T$_1$: 37.5 ± 0.5 T$_2$: 39.0± 0.5	T$_1$: 39.0 ± 0.5 T$_2$: 41.5 ±0.5	T$_2$: 0.45.5± 0.5	T$_2$: 47.5± 0.5	T$_2$: 48 ± 1	T$_2$: 48.5 ± 0.5

Table 1. Second aging temperatures and cooling rate, Hardness, HV_5, volume fraction, $F_V(\alpha_2)$, of the α_2 laths, for all the here studied Ti-46-4 alloy with C from null to 0.5 wt.%.

TEM thin foils were prepared by mechanical grinding and polishing down to a thickness of 0.2-0.3 mm. The 3-mm discs were punched and then dimpled down to a central thickness of 25-30 μm. Final thickness to electron transparency was obtained by twin-jet electro-polishing using a Struers™ Tenupol-5® device with a solution consisting of 5% perchloric acid, 35% butanol, and 60% methanol working at 238K and a voltage V = 24V. Microstructural inspections were carried out by using a Philips™ CM20® electron microscope operating at 200 kV and equipped with a double-tilt specimen holder.

Converged-beam electron diffraction (CBED) was used to determine the lattice parameters of the two phases γ and α_2 with a nominal electron beam of 5-6 nm. The Burgers vector analysis of the partial dislocations was used to distinguish among perfect-twin (Pe-T), pseudo-twin (Ps-T), variant twin (V-T), and overlapping stacking faults. Overlapping stacking faults are recognized by formation of dissimilar partial dislocations on successive planes.

Lamellae spacing was statistically evaluated by ASTM-E112 line intercept method, using a Leika™ Image pro-plus® image analysis software.

Microhardness measurements were carried out at 5 Kg load (HV_5) on polished surfaces and reported values result from averaging at least 7 individual measurements per each experimental condition (*i.e.*, Ti-46-4-C alloy after second aging heat treatment).

3. Results and discussion

3.1. Microstructure modifications induced by the aging treatments (Ti-46Al-4Nb alloy)

Table 1 reports the statistical data measured after second aging treatments (1173 and 1273K) for all the Ti-46-4 alloys with no carbon and with carbon content varying from a minimum of 500 wt. ppm to a maximum of 5000 wt. ppm (0.5%).

The fully lamellar microstructure consisted of equiaxed polycrystalline grains and densely packed lamellae within the grains (**Figure 1 (b)**). The lamellae are composed of α_2 plates between γ twinned phases. The α_2 phase is Ti_3Al with hexagonal close-packed (HCP) lattice and DO_{19} ordered structure. The dominant γ phase is TiAl, with a near-cubic face-centred tetragonal (FCT) $L1_0$ crystal structure (c/a = 1.016). The α_2 plates crystal orientation is such to have the basal plane (0001)-α_2 || close-packed <11-20> directions, that is parallel to the lamellar interface. On the other hand, the γ plates (with four different orientations) share a common close-packed {111} || (0001)-α_2 **[47]**.

Moreover, since there are six possible orientations of γ respect to <11-20>-α_2, the γ/γ interfaces can have a boundary character of one lamella rotation to its neighbour lamellae by a factor of 60° to the (111)-γ crystallographic directions [**45,48**].

Figure 2 shows the lamellae microstructure, their typical length and width, as obtained by aging the intermetallic Ti-48-4 alloy at the two different temperatures of 1173 and 1273K. The width of the plate is not uniform and some interfaces are curved, especially after aging at 1273K. In addition, after aging at 1273K/1h some of the γ plates become thick, while γ/γ interfaces tend to be flat. The lamellae thickening was more pronounced after aging at 1273K respect to aging to a 100K lower temperature (1173K). Thus, the lamellae thickening process was chiefly promoted by rising the second aging temperature. The comparison between the two mean values of lamellae width obtained after annealing at 1173 and 1273K showed that the this reduced slightly from 70 ± 10 to 50 ± 5 nm by 100K temperature increment.

The observed limited width variation induced by rising the second aging temperature was associated with a wider variation of the lamellae size frequency. This is shown by the histograms reported in **Figure 3**. In fact, as reported in **Figure 3**, after annealing at 1173K the lamellae width frequency varied from a minimum of 10 to a maximum of 150 nm, with a peak size frequency of 20 nm. This peak size frequency shifted to 40 nm by aging at 1273K where the width variation was from a minimum of 10 to a maximum size of 250 nm. That is, the size frequency broadened to more than 50% from 1173K to 1273K with a mean size increment of some 40% and a size distribution peak value rise of 20 nm (20 to 40 nm).

On the other hand, for both aging temperatures, the lamellar boundaries are characterized by dense arrays of misfit dislocations with Burgers vectors lying entirely within the interface. This dislocation nature of boundary does reduce the misfit strain energy and improves the interfacial coherency by producing local relaxations [**48-50**]. Annealing also induced a lamellae interface evolution process consisting of trapping of matrix dislocations at the interfaces and their reaction with pre-existing misfit dislocations. This becomes evident by characteristic structures of both tangled dislocations and dislocation loops adjacent to the interfaces. These loops are mostly along (111)-γ planes and are showed in **Figure 4**.

The Burgers vector of the detected loops was identified as $b = 1/2<110]$, and the dislocation loops were reported to form by reactions of interfacial dislocations through misfit dislocations with Burgers vector $b = 1/3<111]$ and Shockley partial dislocations on the (111)-γ interface (see also [**49**]).

Thus, interface reactions between the thin lamellar plates are promoted and driven by the aging temperature. This, in turns, drives the occurrence of the observed lamellar spacing widening. That is, some of the existing interfaces, during second aging treatment are induced to react each other. Thence, thin lamellar plates take place during aging to eventually coarsening the lamellar spacing. Quite similar results were obtained by Yamamoto and co-workers who studied an Ti-48Al-8Nb alloy aged at 1473K/3h [**51**].

The increment of the second aging treatment temperature, from 1173 to 1273K, also induced a twinning interface type evolution. That is, variant-twin (V-T), pseudo-twin (Ps-T), and perfect twin (Pe-T) were formed during aging. **Figure 5** reports representative BF-TEM and high-resolution TEM micrographs showing the peculiar morphology of these three different twin boundaries, i.e., Pe-T, Ps-T, and V-T. The 100K aging increment was found to promote a reduction of number fraction of the variant interface that halved from 1173K to 1273K, and, at the same time, a significant increment of the perfect-twin boundary number fraction. The number fraction of pseudo-twin boundaries and the number fraction of α_2 plates did not vary significantly. **Table 2** shows the statistical data of the number fraction of three different twin boundaries, that is the Pe-T, PsT, and V-T, and the number fraction of the α_2 plate boundaries, after aging at 1173 and 1273K.

It resulted that the lamellar microstructure consisting mostly of the γ/γ interfaces is to some extent thermodynamically stable upon aging up to 1273K. This is also due to the significant α_2/γ boundary number fraction which is promoted by the consisted presence of the thermodynamically stable α_2 lath within the alloy microstructure. Thence, lamellae thermal stability is maintained by aging at 1273K/1h. On the other hand, and in agreement with present results, thermal stability was shown to be maintained up to aging at 1473 K for few minutes in a Ti-48Al alloy containing the thermodynamically stable α_2 laths [**51**]. In fact, the instability of the γ lamellar microstructure is attributed to the microstructure change within lamellae during the early stage of high-temperature aging, especially when the α_2 plates are not present [**51,52**]. The present results also revealed that the twinning interface is induced to assume a perfect-twin boundary character by aging. The perfect-twin is microstructurally and crystallographically characterized by an exact mirror atomic configuration across the interface, whereas pseudo-twin has a quasi-mirror configuration with different atom configurations due to its ordered structure. The variant has the same lattice configuration but different sub-lattice configuration on both sides of the interface [**51**]. It was also observed that the curved interface were induced to line up by the aging temperature. **Figure 6** shows a typical example of the multiple curved interface with triple junction. These interfaces at the triple junction are formed by perfect-twin boundaries (left-hand side respect to the arrows), pseudo-twin boundaries (mostly not visible in the micrographs as they have a slightly different crystallographic orientation), and variant-twin boundaries (right-hand side respect to the arrows).

Table 2 reports the number fraction evolution of V-T, Ps-T, Pe-T and the α_2 phase fraction evolution induced by risisng the second aging temperature by 100K (from 1173 to1273K). On the other hand, by increasing the second annealing temperature, γ laths were induced to grow and more γ laths were induced to nucleate. This microstructure feature did contribute to some extent to the above-mentioned reduction trend of the α_2 lath width, $\lambda_{\alpha 2}$, within the lamellar colonies (**Table 1**).

The influence of the second annealing temperature on the lamellar microstructure modifications was also investigated by Sun [**53**]. He produced ultrafine fully lamellar structures in a Ti-45.3Al-2.1Cr-2Nb reporting that the average interface spacing was increased with annealing temperatures. Sun isothermally aged the alloy for few minutes (<30 min), and then the alloy was maintained close to the equilibrium state favouring coalescence of the γ lamellae. Thence, a larger average lamellae interface spacing respect to the present case was obtained in [**53**].

		1173K	1273K
twin-α_2 number fraction, μm^{-1}	V-T	1.26 ± 0.04	0.68 ± 0.04
	Ps-T	0.42 ± 0.04	0.54 ± 0.03
	Pe-T	0.35 ± 0.03	1.12 ± 0.04
	α_2	0.48 ± 0.02	0.50 ± 0.03

Table 2. Line number fraction, μm^{-1}, of the four different dislocation boundaries: the three existing γ-twin boundaries (Pe-T, Ps-T, and V-T), and the number fraction of the α_2 lath boundaries as measured after aging at 1173K and 1273K.

On the other hand, Park *et al.* [**28**] found that in Ti-46.6Al-1.4Mn-2Mo alloy the interface spacing and the lamellae widths were reduced by a factor of two with 950 wt. ppm carbon addition. They explained this behaviour by carbon segregation at α_2 grain boundaries. This interstitial element segregation was identified as the microstructure feature responsible for the stacking fault energy reduction. This in turns lead to a large number of possible nucleation sites for γ phase formation. This way, on annealing, the γ phase grows at the expense of α_2 resulting in γ lath formation in between the α_2 phase. If the number of γ nucleation sites is increased by carbon, the number of γ lath is expected to be higher and consequently the width of the α_2 laths decreased [**28**].

3.2. Influence of carbon content on the alloy microstructure

The width of the α_2 laths decreased by rising the second annealing temperature, as shown by the experimental data reported in **Figure 3**. The Ti-46Al-4Nb alloy, without carbon additions, the α_2 lath width decreased by ~30%, from 70 to 50 nm. In the carbon-bearing alloy, the width of the α_2 laths after annealing at 1273K steadily remained at a value of $\lambda_{\alpha 2}$ = 25 ± 5 nm up to 2000 wt. ppm of carbon. The α_2 lath reduced slightly to $\lambda_{\alpha 2}$ = 22 ± 4 nm for C ≥ 3000 wt. ppm, that is, as soon as the carbon content reached the lower concentration limit to initiate the formation of the *H*-Ti_2AlC phase, that is at a carbon content of 3000 wt. ppm. In this case, the α_2 lath width slightly widened to remain constant with further C addition to the Ti-46Al-4Nb alloy up to 0.5 wt.% (**Table 3**).

It resulted that, segregation of carbon at the ledges and kinks of α_2/γ interface hinders the thickening of the γ laths and thus leads to finer γ lamellae. Thence, the increased number of nucleation sites and the smaller lath thickening rate are the two keys factor toward the formation of a refined lamellar microstructure in Ti-46Al-4Nb intermetallic alloy with carbon addition.

	Ti-46-4	Ti-46-4+ 500 wt. ppm C	Ti-46-4+ 1000 wt. ppm C	Ti-46-4+ 2000 wt. ppm C	Ti-46-4+ 3000 wt. ppm C	Ti-46-4+ 5000 wt. ppm C
V-T, %	0.24 ± 4	0.22 ± 4	0.20 ± 4	0.17 ± 4	0.12 ± 3	0.05 ± 3
Ps-T, %	0.19 ± 8	0.16 ± 8	0.15 ± 8	0.12 ± 8	0.09 ± 5	0.03 ± 3
Pe-T, %	0.39 ± 8	0.42 ± 6	0.42 ± 5	0.45 ± 4	0.49 ± 3	0.62 ± 3
α_2, %	0.18 ± 4	0.20 ± 4	0.23 ± 4	0.26 ± 4	0.30 ± 3	0.30 ± 3
$\lambda_{\alpha 2}$, nm	25 ± 5	25 ± 5	25 ± 5	25 ± 5	22 ± 4	22 ± 4

Table 3. Normalized number fraction of γ-twin boundaries: V-T, Ps-T, Pe-T, and α_2 lath fraction and boundary spacing as function of C addition to the Ti-46-4 alloy, after second aging at 1273K.

Moreover, carbon content also greatly promoted a redistribution of the different types of twinnings chiefly in favour of the Pe-T number fraction, that passed from 0.39 to 0.62%, that is, it almost double with carbon content up to 0.5 wt.%. It resulted that both V-T and Ps-T reduced markedly by 5 times and 6 times, respectively. Noterwothly, this twininnig character redistribution driven by the carbon content in the Ti-46Al-4Nb alloy recorded a dramatic accelaration at C > 3000 wt.%. As discussed in

the following, at this carbon content the alloy saturated and formation of the carbon-rich *H*-Ti_2AlC phase occurred.

As proposed by Aaronson *et al.* [**54**], transformation by terrace-ledge-kink, in which process compositional fluctuation occurs by jumping of atoms at ledges or kinks at the interphase interface, is favoured by both aging and interstitial addition to TiAl intermetallic alloys. Thence, carbon atoms segregate to the ledges and kinks at interlamellar locations. This in turns is responsible for decreasing the rate of lateral thickening of the γ lamellae. On the other hand, carbon segregation at the grain boundaries induced an increased fault frequency. This, in turns, increased the nucleation rate of the γ phase. The combined effect of increased nucleation rate and decreased thickening rate resulted in the ultrafine character of both α_2 and γ. Moreover, the thermodynamically stable α_2 plates played an important role in pinning the growth of γ grains across the lamellae, as also found in [**55**] where the existence of α_2 laths was found to be responsible for the high thermal stability of the alloy lamellar microstructure.

Figure 7 reports representative micrographs showing the role of carbon on the twinning width and number fraction evolution in the Ti-46-4 alloy aged at 1173 and 1273K. The TEM inspections of the alloy added with 3000 wt. ppm of carbon content showed the presence of small precipitates of *H*-Ti_2AlC phase. These were found homogeneously distributed in the γ phase, and typically formed along dislocation lines. *H* phase particles were elongated with an aspect ratio ranging 5 to 10. The typical size of the *H* particles ranged 40 to 120 nm in equivalent diameter. **Figure 8** is a representative BF-TEM showing the typical morphology and size of the *H*-Ti_2AlC phase that precipitated during second aging at 1273K in the Ti-46-4 alloy with C = 3000 wt. ppm. These particles are lens-shaped with mean equivalent diameter of 300 ± 50 μm. On the other hand, in **[56]** the Ti-48Al intermetallic alloy added with up to 3000 wt. ppm of carbon showed the presence of small *H* phase precipitates, whose mean size was of 50 nm, and homogeneously distributed in the γ phase. The *H*-Ti_2AlC lens-shaped phase has a hexagonal crystallographic structure with cell parameters a =2.977±0.003 Å and c = 13.65±0.01 Å. This is oriented as to have (0001)-*H* || (111)-γ and [11-20]-*H* || [-101]-γ, as also reported in [**57**]. The formation of this phase is driven by the low solubility of carbon within α_2 phase (0.12 at. %) and within γ phase (0.035 at. %) at 700-1000K [**58**].

Menand *et al.* [**58**] showed that, in two-phase Ti intermetallic alloys, the γ phase saturates by interstitial content of ~250 at. ppm, the excess interstitials forming solid solution within the α_2 phase. Precipitation occurs as soon as also the α_2 phase saturates by increasing the amount of the interstitial elements. With this respect, the solubility limit of carbon in α_2 is evaluated at ~3000 wt. ppm (~9600 at. ppm) [**53**].

The statistical evaluation of interlamellar spacing of both γ/α_2 and γ/γ and the related lamellae width showed a clear reduction with alloy carbon contents. A well-defined threshold lower limit was detected and this was identified as C ≅ 3000 wt. ppm.

The present results appeared to be in good agreement with previous findings reported by Perdrix *et al.* [**56**] with a similar intermetallic alloy. In their work, they found that carbon contents from 20 to 1000 wt. ppm induced the α_2 volume fraction, $F_V(\alpha_2)$, to increase and the interlamellar spacing, *IS*, that is, the mean spacing between two consecutive α_2 lamellae to decrease. Perdrix *et al.* [**56**] identified a carbon threshold limit at ~1000 wt. ppm in a Ti-48Al alloy. These trends are similar to those observed in alloys with oxygen [**54**] or nitrogen additions [**55**]. Yet, the transition observed at about 1000 wt. ppm for carbon is higher for nitrogen (3000 wt. ppm) and still higher for oxygen (>6000 wt. ppm) [**48,54-56**]. In the present case, the threshold concentration limit of carbon was found to consisstency higher (C ≅ 3000 wt. ppm) and this is likely to be due to the presence of Nb in the intermetallic alloy and to the second aging temperature (1273K) to which the alloy was subjected. In fact, all the interstitial elements do form a similar *H* phase, when they are added to the intermetallic TiAl alloy above a certain upper cut-off concentration limit. This is different from element to element, but the formation of the *H* phase is anyway favoured. Then, the same crystallographic configuration

and symmetry, with a *H*-Ti_2AlX stoichiometry, where *X* is the specific interstitial element added to the alloy is formed in these interstitial elements added TiAl-based intermetallic alloys.

With this respect, Perdrix *et al.* [**30**] reported the formation of *H*-Ti_2AlN within the γ-phase in an alloy with high nitrogen content. These small lens-shaped precipitation particles were homogeneously distributed within the γ-phase and heterogeneously on dislocations, with particle mean size of 50 nm. In the N-bearing TiAl alloy microhardness was reported to increase linearly for nitrogen amount up to 3000 wt. ppm. For nitrogen contents above 3000 wt. % the hardness remained unchanged irrespectively of the nitrogen content, as the excess of nitrogen started to form *H*-Ti_2AlN particles [**30**].

The here obtained results seem to indicate that carbon, as long as this interstitial element remains in solid solution, promoted α_2 phase stability by increasing $F_V(\alpha_2)$ and decreasing *IS*. On the other hand, whenever carbon solid solution saturates within the α_2 phase, $F_V(\alpha_2)$, and *IS* were reported to remain constant.

In addition, the self diffusion of carbon within the γ-phase is chiefly driven by its diffusion activation energy that is considerably lower than that of niobium. It was also observed that as the carbon content in the alloy rises, the occurrence of perfect-twins (Pe-T) within the alloy microstructure increases significantly. Indeed, the change in the interface character is associated with the difference in interfacial energy among the three types of twin interfaces. In turns, the interfacial energy for each type of twinning can roughly be evaluated by bond energy of atom pair across the interface itslef. On this basis, even if in the present study no calculations were made to determine the alloy stacking fault energy (SFE), it is believed that the increment of Pe-T at the expense of the other partial twins, such as the variant-twins (V-T) and the pseudo-twins (Ps-T), is likely to induce a SFE redcution. This is likely to be the case until carbon does not saturate and the precipitation of a *H*-Ti_2AlC phase occur at the expense of the carbon in solid solution within the γ-grain. Infact, starting from a carbon content above 3000 wt. ppm, the precipitation of the *H*-Ti_2AlC phase occurred progressively draining all the carbon in solid solution within the γ-phase. This, in turns, is likely to further reduce the alloy SFE as the Pe-T recorded a consistent increment at the expense of the Ps-T and the V-T. Yet, to properly address this somehow important issue, further insights are needed. These will have to be using specific and systematic approaches to determine the actual relationship between the different carbon concentration in the C-bearing lamellar Ti-46Al-4Nb alloys and their resulting SFE.

3.3. Correlation between hardness and microstructure

Microhardness, HV_5, seems to follow α_2 volume fraction and the lamellae width reduction trend very closely. With this respect, **Figure 9** shows the $F_V(\alpha_2)$ and HV_5 as a function of the carbon wt. content. The carbon-free alloys aged at 1173K had α_2 lath volume fraction $F_V(\alpha_2)$ = 39% and a hardness of 440 HV_5. The hardness and $F_V(\alpha_2)$ tended to increase by rising the second aging temperature from 1173 to 1273K. This was also observed in a similar studies carried out on a Ti-45Al-7.5Nb alloy by Cha *et al.* [**32**]. As for the influence of carbon, **Figure 9** clearly shows that both $F_V(\alpha_2)$ and HV_5 increased with carbon content from 500 to 5000 wt. ppm, as long as α_2 phase is enriched with carbon as solid solution element. Then the two parameters remain constant as soon as the α_2 phase saturated with carbon and *H*-Ti_2AlC phase precipitates in the γ phase. However, besides this α_2 volume fraction effect, the microhardness of the lamellar alloy is also dependent on the α_2 phase volume fraction. On the contrary, precipitation of the *H*-Ti_2AlC phase does not affect to a significant extent the microhardness. A similar trend of both $F_V(\alpha_2)$ and *HV* was also reported by Perdrix *et al.* in a Ti-48Al intermetallic alloy [**56**].

Moreover, Cam *et al.* [**33**], showed that all interstitial elements stabilize the α_2 phase (that is, C as well as N and O). Both Park *et al.* [**28**] and Cam *et al.* [**33**] reported that the lamellae colony size

was not significantly affected by the addition of less than 3000 at. ppm of carbon (corresponding to 950 wt. ppm), although γ and α_2 lamella mean widths decreased markedly.

Thence, carbon in solid solution increased the microhardness indirectly by increasing $F_V(\alpha_2)$, and directly by increasing the α_2 microhardness contribution given by increasing the carbon amount in solid solution. The latter effect was more effective than the former one. Then, as soon as the α_2 phase saturates with carbon, microhardness and $F_V(\alpha_2)$ no longer varied. On the other hand, low-width α_2 laths resulted in a higher hardness.

According to the Hall–Petch (HP) mechanism, not just high-angle boundaries (grain boundaries) but also all kind of interfaces, *i.e.* in the present case both γ/α_2 and γ/γ, and twinning within the γ phase, act as obstacles for the gliding dislocations. Thus, the HP-dependent alloy mechanical properties are significantly improved whenever the interface density is high, as well as they are greatly improved whenever the grain boundary density is high (that is upon grain size reduction). Similarly, a dislocation strengthening mechanism is also acting in the alloy. The existing dislocations within the lamellae strengthen the alloy by an Orowan-type dislocation mechanism. Consequently, alloy hardness is directly related to the combined Hall-Petch and Orowan strengthening mechanisms primarily through lamellar spacing refinement. Indeed, this issue was already discussed and applied by Kumagai *et al.* [**59**] in a binary Ti-48Al, and by Dehm *et al.* [**60**] in a more complex γ-TiAl based alloy. They both reported quite a similar hardness response to the alloy microstructure lamellae evolution driven by the different applied experimental conditions.

Thence, in order to account to the alloy hardness response driven by the amount of the added carbon content and by the second aging temperature, the two terms, Hall-Petch (HP) and Orowan strengthening, are here discussed. The Orowan relationship is expressed as $HV \cong MGb/\lambda$, where M = 2.8 is the Taylor factor, G is the alloy shear modulus, b the Burgers vector, and λ the mean lamellae width of both γ and α_2. Since, the present alloy is composed by a mixture of two interconnected phases (γ and α_2), a composite-like hardness relationship is here proposed, Eq. (1a):

$$\frac{1}{HV} \cong \frac{f_\gamma}{HV_\gamma} + \frac{f_{\alpha 2}}{HV_{\alpha 2}} \qquad (1a)$$

where f_γ and $f_{\alpha 2}$ are the volume fraction of the γ and α_2 phases, HV_γ and $HV_{\alpha 2}$ are the hardness contributions of each phase, γ and α_2.

Substituting the Orowan relation for each phase, Eq (1a), can be rewritten as, Eq. (1b):

$$\frac{1}{HV} \cong \frac{1}{M}\left[\frac{f_\gamma \lambda\gamma}{G_\gamma b_\gamma} + \frac{f_{\alpha 2}\lambda_{\alpha 2}}{G_{\alpha 2} b_{\alpha 2}}\right] \qquad (1b)$$

In the present study the shear modules were set to $G_\gamma = G_{\alpha 2}$ = 70 GPa, as determined from a theoretical study by Yoo *et al.* in a similar γ/α_2 binary Ti-49Al alloy [**61**]. On the other hand, the tendency of slight increase of the Burgers vector by the carbon solute concentration within the two constituting phases is quite slugghish and the value of b = 0.28 nm of the Ti46Al-4Nb can be considered essentially constant with increasing carbon content. That is, Eq. (1b) can be rewritten as, Eq. (1c):

$$\frac{1}{HV} \cong \frac{f_\gamma \lambda_\gamma + f_{\alpha 2}\lambda_{\alpha 2}}{MGb} \rightarrow HV \cong \frac{MGb}{f_\gamma \lambda_\gamma + f_{\alpha 2}\lambda_{\alpha 2}} \qquad (1c)$$

The variation of both γ laths and α_2 lamellae width with alloy carbon content is reported in **Table 4**. The corresponding alloy strength and the obtained discrepancy with the experimental values coming form the direct hardness measurements is also reported.

The present results clearly show that the hardness increased by reducing the lateral size of the twinning in the γ phase, which actually hinders dislocation sliding. Thence, in ultrafine $\gamma + \alpha_2$ lamellar alloy the hardness resulted to depend on both the α_2 volume fraction and the $\gamma + \alpha_2$ lamellar width. It should be noted that whenever both the γ and α_2 lath widths are in the nano-scale region, the relative volume of the two phases becomes an important parameter. Similarly, in [**32**] hardness increased with both second aging temperature and carbon addition, that is, by reducing the lamellar spacing and γ, α_2 lath widths.

	Ti-46-4	Ti-46-4+ 500 wt. ppm C	Ti-46-4+ 1000 wt. ppm C	Ti-46-4+ 2000 wt. ppm C	Ti-46-4+ 3000 wt. ppm C	Ti-46-4+ 5000 wt. ppm C
λ_γ, nm	50	50	38	36	28	28
$\lambda_{\alpha 2}$, nm	50	48	44	32	26	26
alloy strength from Eq.(1c), MPa	1360	1385	1600	1670	1810	1815
alloy strength from measured *HV*, MPa	1450	1450	1660	1750	1870	1870
discrepancy, %	6	4	4	5	3	3

Table 4. γ twinning width, λ_γ, and α_2 lamellae lath width, $\lambda_{\alpha 2}$, as function of C addition to the Ti-46-4 alloy, after second aging at 1273K.

Perdrix *et al.* [**56**] investigated sub-micrometer- and micrometer-size lamellar microstructures in Ti-48Al alloys with different carbon additions and reported hardness increase with carbon content up to 1.8 at. %. They found α_2 lamellae size ~500 nm irrespective of the carbon content. The α_2 volume fraction increased significantly up to the upper limit of carbon content (0.9 at. %), where precipitation of the *H* phase started. Perdrix *et al.* [**30,56**] seemed to confirm that the hardness is directly correlated to both the α_2 phase amount within the two-phase alloy, and to the solid-solution amount of the interstitial element present within the two-phase microstructure.

As for the validation of the HP relationship reported in Eqs. 1(a)-to-(c), a number of previously published papers accounted on a similar relationship between hardness and lamellar Ti-Al alloy interface spacing [**60,62-64**]. Thus, according to the HP mechanism, interfaces, such as the γ/α_2 and the γ/γ, act as obstacles for the glide of dislocations. Therefore, the HP can still be expressed in the form of the here reported Eqs. 1 (a)-to-(c), since the alloy structure is formed by conventional coarser grains (being in the submicrometer scale well above ~500 nm). That is, an Orowan-type dislocation behavior is acting in the alloy, where dislocations are confined to individual lamellae, which are responsible for a general trend of hardness rise as the lamellar spacing is refined. The hardness increment can be effectively described by HP relationship as shown here. With this respect, Dehm *et al.* [**60**] reported quite a similar phenomenon in a complex Ti-Al based alloy with average interface spacings of ~100 nm. They found that dislocation motion within the γ-phase determines the alloy mechanical properties including hardness, described by a classical HP relationship and taking into consideration the dislocation obstacles constitttuted by the lamellae boundaries.

4. Conclusions

The evolution of γ/γ and γ/α_2 interfaces with carbon addition to a Ti–46Al–4Nb intermetallic alloy was characterized by electron microscopy techniques. The hardness influence on the γ twins and α_2 lamellae widths was also determined. In particular the following major findings can be outlined:

i. Progressive amounts of carbon, from 500 to 5000 wt. ppm, have been added to the Ti-46Al4Nb intermetallic alloy in which a fully lamellar microstructure was obtained by aging at 1273K.

ii. Carbide precipitates of *H*-Ti_2AlC phase appeared to form as soon carbon concentrations in the alloy reached 3000 wt. ppm. The occurrence of *H*-Ti_2AlC phase did not change significantly the lamellar spacing.

iii. Carbon in solid solution increased the α_2 volume fraction and decreases the mean distance between α_2 lamellae upon aging at 1273K.

iv. The carbon content greatly promoted a progressive modification of the different two-phase structure boundaries. The Ti-46Al-4Nb was characterized by an almost equal number fraction presence of variant-twinning, pseudo-twinning, perfect-twin and α_2 lath boundaries Increasing carbon content in the alloy induced a progressive promotion of perfect-twin and α_2 lath boundaries at the expense of the other two types of twin boundaries, variant-twin and pseudo-twin. The formation of the *H*-phase did not constrast this tendency, although it seemed to induce a process saturation.

v. Microhardness increased by solute carbon content in the alloy to reach a saturation limit at C ≅ 3000 wt. ppm, that is as soon as the *H*-phase started to form at the expense of the solute concentration. Correspondingly, the α_2 lath volume fraction followed a similar trend with carbon content and it also saturated whenever carbon reached the alloy solute limit concentration to inititate the precipitation of the *H*-phase out of the excess of solute content. That is, the alloy hardness appeared to strongly depend on the α_2 lamellae width and volume fraction, this,in turns, appeared to be influenced by the second aging temperature and the chemical composition (namely solute carbon content).

Acknowledgments

α

The EU-funded COST Action CA15102 - Soαutions for Critical Raw Materials under Extreme Conditions (CRM-EXTREME), website: https://www.cost.eu/actions/CA15102, is acknowledged for the material supply.

References

[1] Y.W. Kim, Ordered intermetallic alloys, part III: Gamma titanium aluminides, JOM 46 (1994) 30-39.

[2] Y. Yamabe, M. Kikuchi, Report of the 123rd Committee on Heat-Resisting Materials and Alloys, Japan Society for the Promotion of Science, 31 (1990) 179-195.

[3] T. Kawabata, T.T. Abumiya, T. Kanai, O. Izumi, Mechanical properties and dislocation structures of TiAl single crystals deformed at 4.2–293 K, Acta metall. mater. 38 (1990) 1381-1393.

[4] G. Hug, A. Loiseau and A. Lasalmonie, Nature and dissociation of the dislocations in TiAl deformed at room temperature, Phil. Mag. A 54 (1986) 47-65.

[5] J.T. Kandra, E.W. Lee, Temperature and microstructural dependence of the deformation of a high Nb Ti-Al alloy, Metals Mater. Trans. A 25 (1994) 1667-1679.

[6] M.A. Morris, Dislocation configurations in two-phase Ti[sbnd]Al alloys III. Mechanisms producing anomalous flow stress dependence on temperature, Phil. Mag. A 69 (1994) 129-138.

[7] H. A. Lipsitt, D. Shechtman and R. E. Schafrik, The deformation and fracture of TiAl at elevated temperatures, Metall. Trans. A 6 (1975) 1991-1996.

[8] S. A. Court, P. A. Lofvander, M. H. Loretto and H. L. Fraser, The influence of temperature and alloying additions on the mechanisms of plastic deformation of Ti_3Al, Phil. Msg. A 61 (1990) 109-139.

[9] M. Tanimura, Y. Inoue, Y. Koyama, M. Kikuchi, Change in Microstructure during Aging at 1273K in Ti-40at.%Al alloy, Mater. Trans JIM 37 (1996) 1190-1196.

[10] Yamabe Y, Takeyama M, Kikuchi, Microstructure evolution through solid-solid phase transformations in gamma titanium aluminides, In: Kim YW, Wagner R, Yamaguchi H, editors. Gamma titanium aluminides. Annual meeting and exhibition of the Minerals, Metals and Materials Society (TMS), Las Vegas, NV (United States), 12-16 Feb 1995, TMS, (1995) 111-118.
[11] Y.W. Kim, Effects of microstructure on the deformation and fracture of γ-TiAl alloys, Mater. Sci. Eng. A 192-193 (1995) 519-533.
[12] W. Schillinger, H. Clemens, G. Dehm, A. Bartels, Microstructural stability and creep behavior of a lamellar γ-TiAl based alloy with extremely fine lamellar spacing, Intermetallics 10 (2002) 459-466.
[13] P.J. Maziasz, C.T. Liu, Development of ultrafine lamellar structures in two-phase γ-TiAl alloys, Metall. Mater. Trans. A 29 (1998) 105-117.
[14] H. Zhu, J. Matsuda, K. Maruyama, Influence of heating rate in α + γ dual phase field on lamellar morphology and creep property of fully lamellar Ti-48Al alloy, Mater. Sci. Eng. A 397 (2005) 58-64.
[15] Y.Q. Sun, Surface relief and the displacive transformation to the lamellar microstructure in TiAl, Phil. Mag.Lett. 78 (1998) 297-305.
[16] Y.Q. Sun, Nanometer-scale, fully lamellar microstructure in an aged TiAl-based alloy, Metall. Mater. Trans. A 29 (1998) 2679-2685.
[17] H. Clemens, A. Bartels, S. Bystrzanowski, H. Chladil, H. Leitner, G. Dehm G, R. Gerling, F.P. Schimansky, Grain refinement in γ-TiAl-based alloys by solid state phase transformations, Intermetallics 14 (2006) 1380-1385.
[18] W. Lefebvre, A. Menand, A. Loiseau, Influence of oxygen on phase transformations in a Ti-48 At. pct Al alloy, Metall. Mater. Trans. A 34 (2003) 2067-2075.
[19] Y.W. Kim, Microstructural evolution and mechanical properties of a forged gamma titanium aluminide alloy, Acta Metall. Mater. 40 (1992) 1121-1134.
[20] R.V. Ramanujan, P.J. Maziasz, The mechanism of formation of a fine duplex microstructure in Ti-48Al-2Mn-2Nb alloys, Metall. Mater. Trans. A 27 (1996) 1661-1673.
[21] C.T. Liu, J.H. Schneibel, P.J. Maziasz, J.L. Wright, D.S. Easton, Tensile properties and fracture toughness of TiAl alloys with controlled microstructures, Intermetallics 4 (1996) 429-440.
[22] H. Zhu, J. Matsuda, K. Maruyama, Microstructural refinement mechanism by controlling heating process in multiphase materials with particular reference to γ-TiAl, Appl. Phys. Lett. 88 (2006) 131908.
[23] W.H. Tian, M. Nemoto, Effect of carbon addition on the microstructures and mechanical properties of y-TiAl alloys, Intermetallics 5 (1997) 237-244.
[24] S.J. Yang, S.W. Nam, Investigation of α2/γ phase transformation mechanism under the interaction of dislocation with lamellar interface in primary creep of lamellar TiAl alloys, Mater. Sci. Eng. A 329-331 (2002) 898-905.
[25] G. Cao, L. Fu, J. Lin, Y. Zhang, C. Chen, The relationships of microstructure and properties of a fully lamellar TiAl alloy, Intermetallics 8 (2000) 647-653.
[26] M. Perez-Bravo, I. Madariaga, K. Ostolaza, M. Tello, Microstructural refinement of a TiAl alloy by a two step heat treatment, Scripta Mater. 53 (2005) 1141-1146.
[27] M. Beschliesser, A. Chatterjee, A. Lorich, W. Knabl, H. Kestler, G. Dehm, H. Clems, Designed fully lamellar microstructures in a γ-TiAl based alloy: adjustment and microstructural changes upon long-term isothermal exposure at 700 and 800 °C, Mater. Sci. Eng. A 329-311 (2002) 124-129.
[28] H.S. Park, S.W. Nam, N.J. Kim, S.K. Hwang, Refinement of the lamellar structure in TiAl-based intermetallic compound by addition of carbon, Scripta Mater. 41 (1999) 1197-1203.
[29] H. Zhong, Y. Yang, J. Li, J. Wang, T. Zhang, S. Li, J. Zhang, Influence of oxygen on microstructure and phase transformation in high Nb containing TiAl alloys, Mater. Letters 83 (2012) 198-201.
[30] F. Perdrix, M.-F. Trichet, J.-L. Bonnentien, M. Cornet, J. Bigot, Influence of nitrogen on the microstructure and mechanical properties of Ti-48Al alloy, Intermetallics 19 (2001) 147-155.

[31] H.S. Cho, S.W. Nam, J.H. Yun, D.M. Wee, Effect of 1 at.% nitrogen addition on the creep resistance of two phase TiAl alloy, Mater. Sci. Eng. A 262 (1999) 129-136.
[32] L. Cha, C. Scheu, H. Clemens, H.F. Chladil, G. Dehmb, R. Gerling, A. Bartels, Nanometer-scaled lamellar microstructures in Ti-45Al-7.5Nb-(0; 0.5)C alloys and their influence on hardness, Intermetallics 16 (2008) 868-875.
[33] G. Cam, H.M. Flower, D.R.F. West, The alloying of titanium aluminides with carbon. High-Temperature Ordered Intermetallic Alloys III MRS Proceedings, 133 (1988) 663-669.
[34] D.S. Shih, R.A. Amato, interface reaction between Gamma-TiAl alloys and reinforcement, Scripta Metall. Mater. 24 (1990) 2053-2058.
[35] Y.W. Kim, D.M. Dimiduk, Progress in the understanding of gamma titanium aluminides, JOM 43 (1991) 40-47.
[36] S. Djanarthany, C. Servant, R. Penelle, Influence of an increasing content of molybdenum on phase transformations of Ti-Al-Mo aluminides - relation with mechanical properties, Mater. Sci. Eng. A 152 (1992) 48-53.
[37] S.G. Pyo, Y.W. Chang, N.J. Kim, Microstructure and mechanical properties of duplex TiAl alloys containing Mn, Met. Mater. 1 (1995) 107-115.
[38] P.D. Crofts, P. Bowen, I.P. Jones, The effect of lamella thickness on the creep behavior of Ti-48Al-2Nb-2Mn, Scripta Metall. Mater. 35 (1996) 1391-1396.
[39] S.G. Pyo, S.M. Choi, M.S. Yoo, J.K. Oh, S.K. Whang, N.J. Kim, Nucleation and growth of α phase in hot extruded Ti-46.6Al-2Mo-1.4Mn intermetallic alloy produced by hot extrusion of elemental powders, Mater. Sci. Eng. A 374 (2004) 160-169.
[40] A. Denquin, S. Naka, Phase transformation mechanisms involved in two-phase TiAl-based alloys-I. Lambellar structure formation, Acta Metall. 44 (1996) 343-352.
[41] A. Denquin, S. Naka, Phase transformation mechanisms involved in two-phase TiAl-based alloys-II. Discontinuous coarsening and massive-type transformation, Acta Metall. 44 (1996) 353-365.
[42] K.S. Chan, J. Onstott, K.S. Kumar, The fracture resistance of a binary TiAl alloy, Met. Trans. A 31 (2000) 71-80.
[43] S. Zghal, S. Naka, A. Couret, A quantitative TEM analysis of the lamellar microstructure in TiAl based alloys, Acta Metall. 45 (1997) 3005-3015.
[44] W.J. Zhang, L. Francesconi, E. Evangelista, G.L. Chen, Characterization of widmanstätten laths and interlocking boundaries in fully-lamellar TiAl-base alloy, Scripta Mater. 37 (1997) 627-633.
[45] M. Yamaguchi, Y. Umakoshi, The deformation behaviour of intermetallic superlattice compounds, Progr. Mater. Sci. 34 (1990) 1-148.
[46] F. Appel, M. Oehring, J.D.H. Paul, C. Klinkenberg, T. Carneiro, Physical aspects of hot-working gamma-based titanium aluminides, Intermetallics 12 (2004) 791-802.
[47] Y.Q. Sun, Nanometer-Scale, Fully Lamellar Microstructure in an Aged TiAl-Based Alloy, Metall. Mater. Trans. A 29 (1998) 2679-2685.
[48] B.K. Kad, P.M. Hazzledine, Shear boundaries in lamellar TiAl, Phil. Mag. Lett. 66 (1992) 133-139.
[49] F. Appel, R. Wagner, Microstructure and deformation of two-phase γ-titanium aluminides, Mater. Sci. Eng. R 22 (1998) 187-268.
[50] H. Inui, A. Nakamura, M.H. Oh, M. Yamaguchi, High-resolution electron microscope study of lamellar boundaries in Ti-rich TiAl polysynthetically twinned crystals, Ultramicroscopy 39 (1991) 268-278.
[51] Y. Yamamoto, M. Takeyama, T. Matsuo, Stability of lamellar microstructure consisting of γ/γ interfaces in Ti–48Al–8Nb single crystal at elevated temperatures, Mater. Sci. Eng. A 329-331 (2002) 631-636.
[52] H. Inui, M.H. Oh, A. Nakamura, M. Yamaguchi, Ordered domains in tial coexisting with ti3al in the lamellar structure of ti-rich tial compounds, Phil. Mag. A 66 (1992) 539-555.

[53] Y.Q. Sun, Nanometer-scale, fully lamellar microstructure in an aged TiAl-based alloy, Metall. Mater. Trans. A 29 (1998) 2679-2685.
[54] H. I. Aaronson, Atomic mechanisms of diffusional nucleation and growth and comparisons with their counterparts in shear transformations, Metall. Trans. A 24 (1993) 241-276.
[55] D. Blavette, P. Duval, L. Letellier, M. Guttmann, Atomic-scale APFIM and TEM investigation of grain boundary microchemistry in Astroloy nickel base superalloys, Acta Mater. 44 (1996) 4995-5005.
[56] F. Perdrix, M.-F. Trichet, J.-L. Bonnentien, M. Cornet, J. Bigot, Relationships between interstitial content, microstructure and mechanical properties in fully lamellar Ti-48Al alloys, with special reference to carbon, Intermetallics 9 (2001) 807-815.
[57] W. H. Tia, M. Nemoto, Effect of carbon addition on the microstructures and mechanical properties of y-TiAl alloys, Intermetallics 5 (1997) 237-244.
[58] A. Menand, A. Huguet, A. Nérac-Partaix, Interstitial solubility in γ and α_2 phases of TiAl-based alloys, Acta Mater. 44 (1996) 4729-4737.
[59] T. Kumagai, E. Abe, M. Takeyama, M. Nakamura, Microstructural evolution of massively transformed γ-TiAl during isothermal aging, Scripta Mater 36 (1997) 523-529.
[60] G. Dehm, C. Motz, C. Scheu, H. Clemens, P. Mayrhofer, C. Mitterer, Mechanical size-effects in miniaturized and bulk materials, Adv. Eng. Mater. 8-11 (2006) 1033-1045.
[61] M.H. Yoo, J. Zou, C.L. Fu, Mechanistic modeling of deformation and fracture behavior in TiAl and Ti_3Al, Mater. Sci. Eng. A 192-193 (1995) 14-23.
[62] F. Appel, R. Wagner, Microstructure and deformation of two-phase γ-titanium aluminides. Mater. Sci. Eng. R 22 (1998) 187-268.
[63] Y.W. Kim, Strength and ductility in TiAl alloys. Intermetallics 6 (1998) 623-628.
[64] D.M. Dimiduk, P.M. Hazzeldine, T.A. Parthasarathy, S. Seshagiri, M.G. Mendiratta, The role of grain size and selected microstructural parameters in strengthening fully lamellar TiAl alloys. Metall. Mater. Trans. A 29 (1998) 37-47.

Figures captions

Figure 1. Schematic representation of the heat treatments to which the alloys were subjected, a), LM-BF TEM showing the two-phase alloy microstructure (Ti-46-4 aged at T_1 = 1173K), b). Insets in b) report indexed SAEDPs for the two-phase identification: α_2 HCP-[01-10], and γ FCT-[001].

Figure 2. Lamellar microstructure of the Ti-46-4 alloy for both second aging temperatures T_1 = 1173K, a), and T_1 = 1273K, b). The size distribution of the lamellae width after both second aging temperatures are reported in **Table 1**. These ranged 10 to 150 nm, after 1173K, and 10 to 250 nm, after 1273K.

Figure 3. Distribution of lamellae width of the Ti-46-4 alloy for both second aging temperatures T_1 = 1173K (white-dashed bars), and T_1 = 1273K (grey-coloured bars). The mean lamellae width (spacing) is reported in the histograms.

Figure 4. Dislocation loops formed upon second annealing on (111)-γ planes (Ti-46-4 annealed at 1273K).

Figure 5. BF-TEM of perfect twins (Pe-T), a), HR-TEM showing Pe-T atomic arrangements, b), pseudo-twins (Ps-T), c), and HR-TEM showing atomic arrangements of Pe-T and Ps-T with variant-twins (V-T), d). In b) lines represent the atomic alignment of Pe-T and eventually Ps-T, V stands for V-T and is placed where atomic variant dis-alignment is present in the micrograph. SAEDP recorded at the triple junction of Pe-T, Ps-t and V-T of d) is also reported in the inset. All micrographs refer to Ti-46-4 annealed at 1273K.

Figure 6. BF-TEM of Ti-48-4 alloy aged at 1273K showing multiple triple junctions (indicated by arrows in the figure) characterized by the formation curved variant of twin boundaries: perfect-twin (Pe-T), pseudo-twin (PsT), and the variant twin (V-T) after aging at 1273K.

Figure 7. Representative BF-TEM showing the role of C on the twinning width and number fraction evolution; Ti-46-4 with C = 500 wt. ppm, a), C = 1000 wt. ppm, b), C = 2000 wt. ppm, c), C = 3000 wt. ppm, d), C = 5000 wt. ppm, e). All micrographs refer to second aging at 1273K.

Figure 8. BF-TEM of *H*-Ti_2AlC phase (Ti-46-4 aged at 1273K).

Figure 9. *H* and $F_V(\alpha_2)$ vs. C (wt. ppm) content.

Highlights

- evolution of γ/γ and γ/α_2 interfaces in Ti–46Al–4Nb driven by Carbon addition;
- *H*-Ti_2AlC phase formed at C > 3000 wt. ppm;
- formation of *H*-Ti_2AlC did not change α_2 lamellar spacing;
- Carbon increased α_2 volume fraction and decreased mean α_2 lamellae width;
- Carbon influenced the number fraction of variant-twinning, pseudo-twinning, perfect-twin and α_2 lath boundaries;
- Hardness depended on Carbon content, α_2 lamellae width and volume fraction, and *H* phase formation.

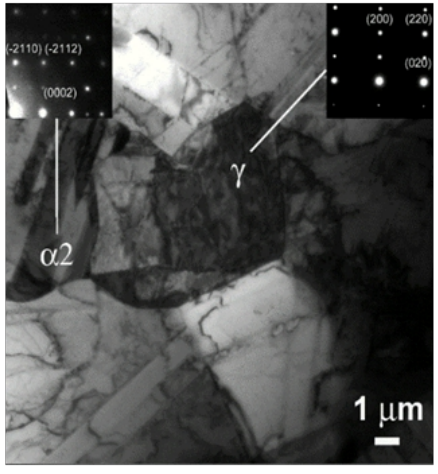

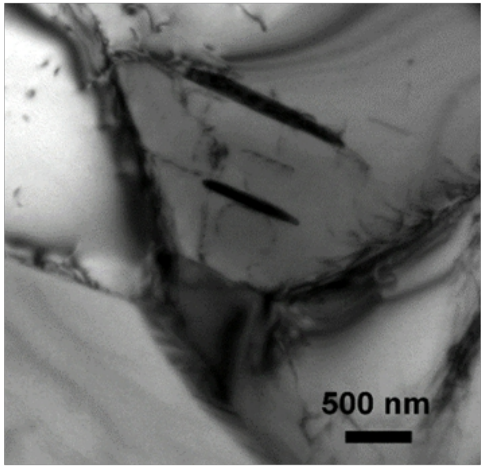

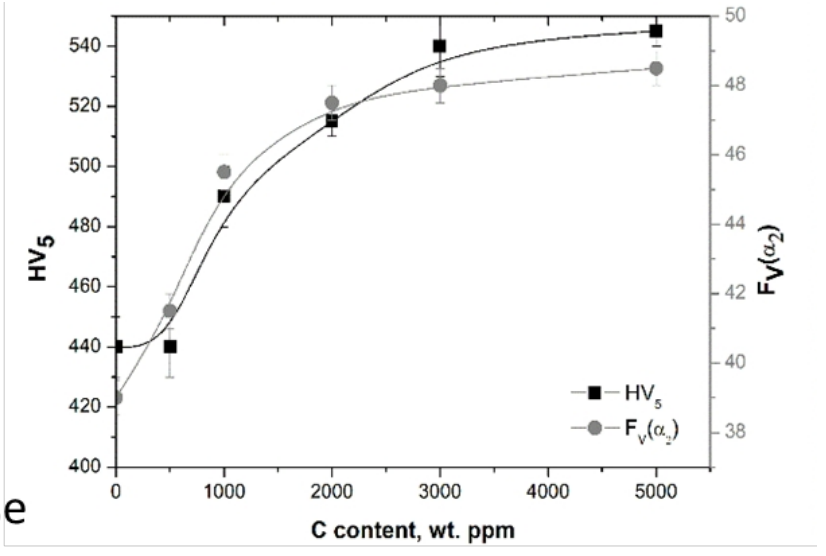

formation of *H*-Ti_2AlC phase
starting from C = 3000wt. ppm

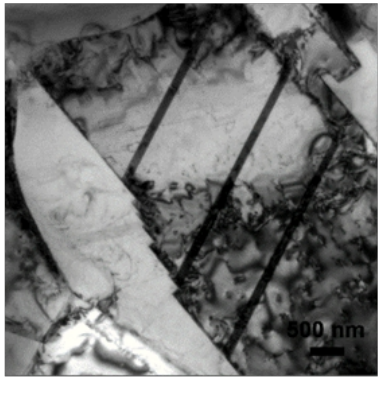

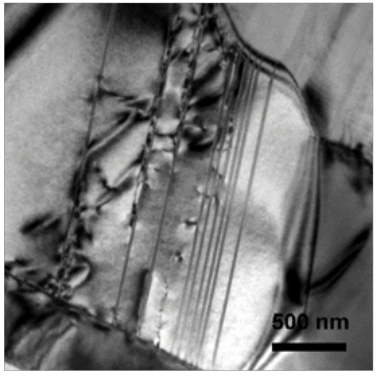

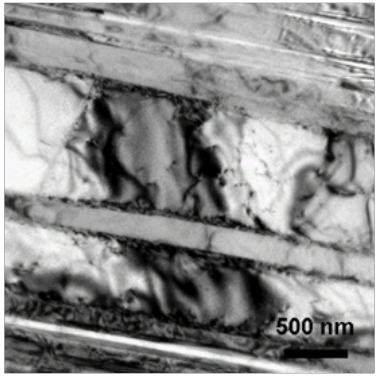

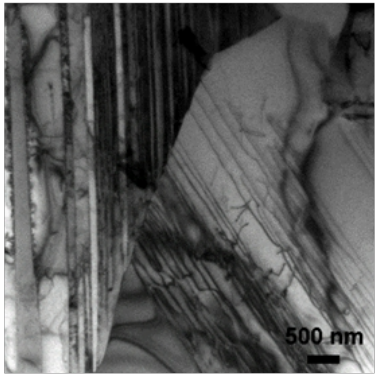

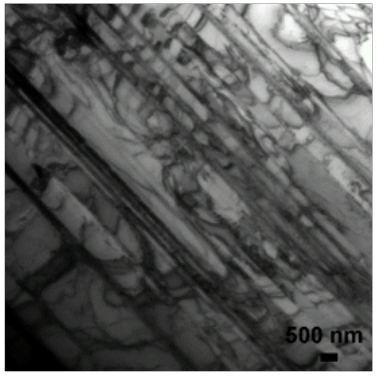

C from 500 to 5000 wt. ppm: γ-twin and α2 lateral width reduction

& variant-twin, pseudo-twin, perfect-twin, α2 lath boundary number fraction modifiaction

Carbon content driven high temperature γ-α_2 interface modifications and stability in Ti-46Al-4Nb intermetallic alloy

Marcello Cabibbo

DIISM / Università Politecnica delle Marche, Via Brecce Bianche 12, 60131-Ancona, Italy.

Abstract.

The effect of carbon addition on the microstructure modifications and hardness response of a two-phase lamellar Ti-46Al-4Nb intermetallic alloy was studied. The alloy was heat treated as to have an initial tow-phase refined lamellar microstructure consisitng of α_2 laths and γ phase characterized by nanometric wide twinning. The effect of carbon in solid solution in the α_2 phase and the onset of the *H*-Ti_2AlC phase precipitation within the γ phase was addressed. A threshold carbon limit of C ≅ 3000 wt. ppm was identified as lower limit solute concentration for the precipitation initiation of the *H* phase particles. The major alloy hardening factors were identified as the refined interlamellar spacing, the fine twinning and the amount of carbon in solid solution. The role of *H* phase formation on the alloy hardening with carbon content was addressed and it was essentially such to induce a hardening saturation effect.

Keywords: TiAl intermetallic alloy; interstitial elements; γ-lamellae interface; twinning; transmission electron microscopy.

1. Introduction

The class of γ titanium aluminides are very interesting materials for structural use at elevated temperatures owing to their high specific strength, low density and good oxidation resistance [**1,2**]. These alloys have excellent properties compared to other high-temperature resistant metallic materials, such as Ni- and Co-based superalloys. In particular, two phase γ-TiAl based alloys with a fully lamellar structure have attracted significant interest due to their outstanding creep resistance and fracture toughness [**3-6]**

The typical microstructure of this class of alloys consists of alternating α_2-lamellae and γ-plates, which are formed during cooling from the parent α phase. The mutual crystallographic relationship is as (0001)-α_2 || (111)-γ and <1120>-α_2 || <110>-γ [**3**]. The γ-TiAl has a $L1_0$ face-centred tetragonal (FCT) crystal structure with lattice parameters a = 0.4005 nm and c = 0.4070 nm. The primary deformation modes of the γ phase are <110> slip and {111}<112> twinning [**7**]. The α_2 Ti_3Al phase has a DO_{19} hexagonal close-packed (HCP) crystal structure with lattice parameters a = 0.579 nm and c = 0.467 nm. Ti_3Al preferentially deforms in the prismatic {10-10}1/6<11-20> slip directions, the basal {0001}1/6<11-20> directions, and the pyramidal {10-2-1}1/6<11-26> directions [**8**].

This duplex microstructure improves the alloy ductility, while, the lamellar structure promotes fracture toughness and creep resistance [**9**]. In particular, a number of factors influence the lamellar structure and the resulting alloy mechanical properties [**10**]. These are the α_2 volume fraction, $F_V(\alpha_2)$, the α_2 lamellae width, $L_{\alpha 2}$, and the lamellae spacing, S_l. It is well known that the lamellae spacing is a dominant factor influencing the alloy hardness, as this increases by decreasing the lamellae spacing [**11**]. With this regards, Schillinger *et al.* [**12**] showed that ultrafine lamellae improve the short-term creep behavior of Ti–46Al-1.5Cr–2Mo–X alloys. Thus, different heat

treatments and alloying elements were applied in γ-TiAl based alloys to drive and control the lamellae spacing in fully lamellar structures [**11,13-16**]. Recently, using multistep heat treatments, Clemens *et al.* [**17**] reported on successfully refined fully lamellar structures in different γ-TiAl based alloys. Usually, lamellar structures can form by one of the following two kinds transformation sequence induced by heat treatment: $\alpha - (\alpha+\gamma) - (\alpha_2+\gamma)$, or $\alpha - \alpha_2 - (\alpha_2+\gamma)$ [**18**]. These two reactions actually correspond to a different lamellar structure, as in the first case the alloy is characterized by a conventional lamellar structure, that is, lamellae with usual width, $L_{\alpha 2}$. On the contrary, in the second case, ultrafine lamellar structures are induced to form.

For usual lamellar microstructures different researchers studied the role of heat treatment, alloying elements and other microstructure features on the lamellae formation mechanisms in γ-Ti-Al based alloys [**13,19-27**]. Other research works addressed the microstructure and mechanical characterization of ultrafine lamellar structure Ti-Al based alloys [**15,16,18**]. It resulted that understanding the factors affecting the lamellae width, $L_{\alpha 2}$ and their thermal stability, both in terms of alloying elements (Nb being one of the most important element in such alloys) and in terms of specific heat treatments is a key issue in Ti-Al based intermetallic alloys. Among the different usually added elements, carbon and the other interstitial elements, along with heat treatments, is known to significantly modify both lamellae width $L_{\alpha 2}$, and spacing, S_l, and their thermal stability and character. With this regard, studies on the effects of all interstitial elements, such O, N, C, on the microstructure modifications and the mechanical properties of the Ti-Al alloys were published in several contributions. In particular, in the TiAl γ phase the solubility of O, N or C is low, and then precipitate particles tend to form by both prolonged heat treatments and interstitial content. On the other hand, the interstitial elements have high solubility within the hexagonal α_2 phase. Thus, strong interactions among the existing interstitital elements within the matrix, the sliding dislocations induced during plastic deformation, and the existing particles characterize the mechanical response of such interstitial-bearing alloys **[28].**

Upon high temperature and cooling treatment sequences of Ti-Al lamellar-structured alloys, lamellae interfaces are not only of the type α_2/γ but also many γ/γ interfaces are also present, since during alloy cooling, the fraction of γ plates is induced to rise up to values for which γ interfaces start to meet. Moreover, γ/γ interfaces can be crystallographically classified into three different types; variant interface twin (V-T), perfect-twin (Pe-T), and pseudo-twin (Ps-T) boundaries [**2,9,10**]. Thus, the alloy thermal stability is likely to chiefly depends on the stability and character of both the α_2/γ and the γ/γ interfaces.

The addition of a ternary element to the Ti-Al alloy, such as Cr, Mn, V, and Nb is considered necessary to improve the room-temperature ductility and fracture toughness of the two-phase Ti-Al intermetallic alloys [**28-31**]. Both mechanical properties are usuually improved by microstructural induced modifications and by solute elements driven slip and twin deformation [**32-37**]. In particular, the addition of Nb makes the α to γ transformation kinetics sluggish **[37,38]**. By a microstructure viewpoint Nb addition in the two phase Al-Ti alloys distributes equally into α and γ phases. Thence, no segregation of Nb takes place at the lamellae interface boundaries. That is, the Nb addition in the alloy does not influence the stability among the different lamellae interfaces [**38**].

Following the here reported state of the art, this study focuses on the role of different amount of carbon addition on the lamellae morphology and twining character in a two-phase ternary Ti-46Al-4Nb intermetallic alloy. In particular, the influence of the heat treatment, namely two aging temperatures, was addressed to determine the lamellae stability and the twin interface character in the Ti-Al-Nb added with increasing amount of carbon, from a minimum of (wt.%) C = 500 ppm, to a maximum of 5000 ppm (C=0.5%).

2. Experimental details

In this study an Ti-46Al-4Nb (Ti-46-4) alloy added with different amount of carbon was used. **Table 1** reports the alloy chemical composition, the exact amounts of the interstitial element (C) added to the alloy, and the two different thermal treatments to which all the C-modified Ti-46-4 intermetallic alloys were subjected.

The alloys were prepared by powder metallurgy (PM) and a homogeneous chemical distribution of the substitutional elements (Al, Nb) was obtained. Initial powdered material was compacted by hot-isostatic pressing at 1573K, 170 MPa, for a total duration of 4 h, and then cooled at a rate of 20K/min. Lamellar microstructure was obtained by rapidly cooling the single-phase hexagonal α phase alloy from 1573K through the temperature range of 1523 to 1473K [**39**]. Ultrafine lamellar microstructure consisting of $\gamma + \alpha_2$ phases was obtained by a two-step heat treatment. The first step of the heat treatment consisted of heating above the $T_{\alpha\text{-transus}}$ temperature (1423K/1h) [**40**], followed by oil quenching (OQ) to room temperature (RT) at a cooling rate sufficiently rapid to suppress the α to $\alpha + \gamma$ to $\alpha_2 + \gamma$ transformation. That is, a direct α to α_2 transformation was induced. The second step consisted on heating the alloys to 1173 or 1273K at a rate of 25K/min, immediately followed by OQ. This two-step heat treatment was able to induced the formation of an ultrafine lamellar structure.

TEM thin foils were prepared by mechanical grinding and polishing down to a thickness of 0.2-0.3 mm. The 3-mm discs were punched and then dimpled down to a central thickness of 25-30 μm. Final thickness to electron transparency was obtained by twin-jet electro-polishing using a Struers™ Tenupol-5® device with a solution consisting of 5% perchloric acid, 35% butanol, and 60% methanol working at 238K and a voltage V = 24V. Microstructural inspections were carried out by using a Philips™ CM20® electron microscope operating at 200 kV and equipped with a double-tilt specimen holder.

Converged-beam electron diffraction (CBED) was used to determine the lattice parameters of the two phases γ and α_2 with a nominal electron beam of 5-6 nm. The Burgers vector analysis of the partial dislocations was used to distinguish between true twin, pseudo-twin, variant twin, and overlapping stacking faults. Overlapping stacking faults are recognized by formation of dissimilar partial dislocations on successive planes.

Lamellae spacing was statistically evaluated by ASTM-E112 line intercept method, using a Leika™ Image pro-plus® image analysis software.

Microhardness measurements were carried out at 5 Kg load (HV_5) on polished surfaces and reported values result from averaging at least 7 individual measurements per each experimental condition (*i.e.*, Ti-46-4-C alloy after second aging heat treatment).

	Ti-46-4	Ti-46-4-C_1	Ti-46-4-C_2	Ti-46-4-C_3	Ti-46-4-C_4	Ti-46-4-C_6
Chemical composition, wt.%	46Al, 4Nb	46Al, 4Nb, C(500ppm)	46Al, 4Nb, C(1000ppm)	46Al, 4Nb, C(2000ppm)	46Al, 4Nb, C(3000ppm)	46Al, 4Nb, C(5000ppm)
2nd heating T, K/h	T_1=1173/1 cooling 15K/min T_2=1273/1 cooling 25K/min	T_1=1173/1 cooling 15K/min T_2=1273/1 cooling 25K/min	T_2=1273/1 cooling 25K/min	T_2=1273/1 cooling 25K/min	T_2=1273/1 cooling 25K/min	T_2=1273/1 cooling 25K/min
Hardness, HV_5	T_1:410±10 T_2:440±10	T_1:420±10 T_2:440±10	T_2:490±10	T_2:515±5	T_2:540±10	T_2:545±5
$F_V(\alpha_2)$, %	T_1: 37.5 ± 0.5 T_2: 39.0± 0.5	T_1: 39.0 ± 0.5 T_2: 41.5 ±0.5	T_2: 0.45.5± 0.5	T_2: 47.5± 0.5	T_2: 48 ± 1	T_2: 48.5 ± 0.5

Table 1. Second aging temperatures and cooling rate, Hardness, HV_5, volume fraction, $F_V(\alpha_2)$, of the α_2 laths, for all the here studied Ti-46-4 alloy with C from null to 0.5 wt.%.

3. Results and discussion

3.1. Microstructure modifications induced by the aging treatments (Ti-46Al-4Nb alloy)

Table 1 reports the statistical data measured after second aging treatments (1173 and 1273K) for all the Ti-46-4 alloys with no C and with C content varying from a minimum of 300 wt. ppm to a maximum of 5000 wt. ppm (0.5%).

The fully lamellar microstructure consisted of equiaxed polycrystalline grains and densely packed lamellae within the grains (**Figure 1**). The lamellae are composed of α_2 plates between γ twinned phases. The α_2 phase is Ti_3Al with hexagonal close-packed (HCP) lattice and DO_{19} ordered structure. The dominant γ phase is TiAl, with a near-cubic face-centred tetragonal (FCT) $L1_0$ crystal structure (c/a = 1.016). The α_2 plates crystal orientation is such to have the basal plane (0001)-α_2 || close-packed <11-20> directions, that is parallel to the lamellar interface. On the other hand, the γ plates (with four different orientations) share a common close-packed {111} || (0001)-α_2 **[41]**.

Moreover, since there are six possible orientations of γ respect to <11-20>-α_2, the γ/γ interfaces can have a boundary character of one lamella rotation to its neighbour lamellae by a factor of 60° to the (111)-γ crystallographic directions [**39,42**].

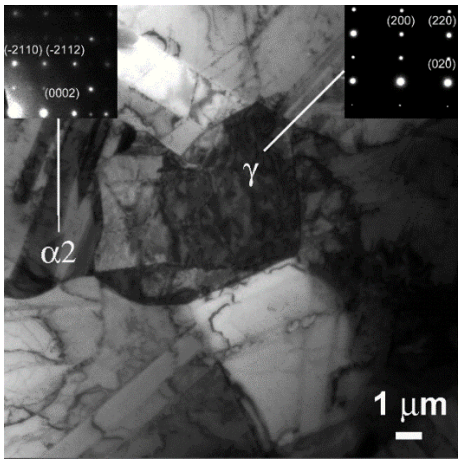

Figure 1. LM-BF TEM showing the two-phase alloy microstructure (Ti-46-4 aged at T_1 = 1173K). Insets report indexed SAEDPs for the two-phase identification: α_2 HCP-[01-10], and γ FCT-[001].

Figure 2 shows the lamellae microstructure, their typical length and width, as obtained by aging the intermetallic Ti-48-4 alloy at the two different temperatures of 1173 and 1273K. The width of the plate is not uniform and some interfaces are curved, especially after aging at 1273K. In addition, after aging at 1273K/1h some of the γ plates become thick, while γ/γ interfaces tend to be flat. The lamellae thickening was more pronounced after aging at 1273K respect to aging to a 100K lower temperature (1173K). Thus, the lamellae thickening process was chiefly promoted by rising the second aging temperature. The comparison between the two mean values of lamellae width obtained after annealing at 1173 and 1273K showed that the this reduced slightly from 70 ± 10 to 50 ± 5 nm by 100K temperature increment.

The observed limited width variation induced by rising the second aging temperature was associated with a wider variation of the lamellae size frequency. This is shown by the histograms reported in **Figure 3**. In fact, as reported in **Figure 3**, after annealing at 1173K the lamellae width frequency varied from a minimum of 10 to a maximum of 150 nm, with a peak size frequency of 20 nm. This peak size frequency shifted to 40 nm by aging at 1273K where the width variation was from a minimum of 10 to a maximum size of 250 nm. That is, the size frequency broadened to more

than 50% from 1173K to 1273K with a mean size increment of some 40% and a size distribution peak value rise of 20 nm (20 to 40 nm).

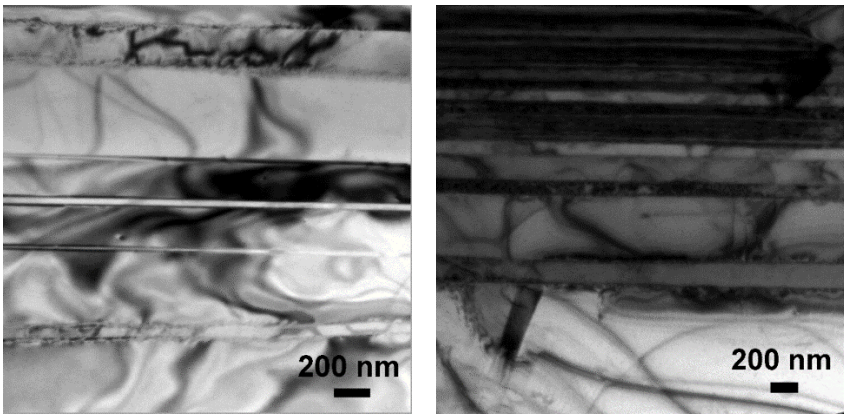

a) b)

Figure 2. Lamellar microstructure of the Ti-46-4 alloy for both second aging temperatures T_1 = 1173K, a), and T_1 = 1273K, b). The size distribution of the lamellae width after both second aging temperatures are reported in **Table 1**. These ranged 10 to 150 nm, after 1173K, and 10 to 250 nm, after 1273K.

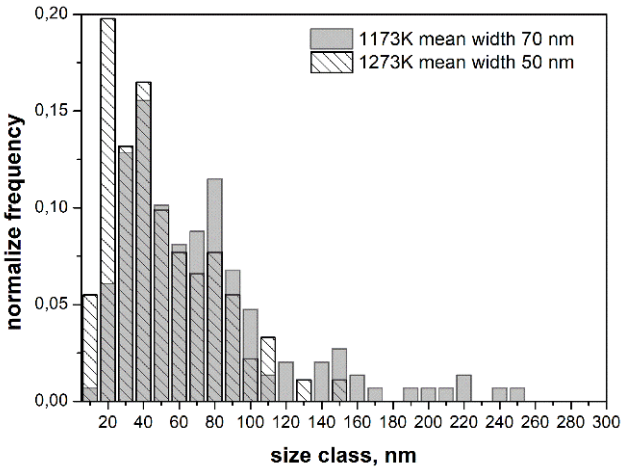

Figure 3. Distribution of lamellae width of the Ti-46-4 alloy for both second aging temperatures T_1 = 1173K (white-dashed bars), and T_1 = 1273K (grey-coloured bars). The mean lamellae width (spacing) is reported in the histograms.

On the other hand, for both aging temperatures, the lamellar boundaries are characterized by dense arrays of misfit dislocations with Burgers vectors lying entirely within the interface. This dislocation nature of boundary does reduce the misfit strain energy and improves the interfacial coherency by producing local relaxations [**42-44**]. Annealing also induced a lamellae interface evolution process consisting of trapping of matrix dislocations at the interfaces and their reaction with pre-existing misfit dislocations. This becomes evident by characteristic structures of both tangled dislocations and dislocation loops adjacent to the interfaces. These loops are mostly along (111)-γ planes and are showed in **Figure 4**.

The Burgers vector of the detected loops was identified as b = 1/2<110], and the dislocation loops were reported to form by reactions of interfacial dislocations through misfit dislocations with Burgers vector b = 1/3[111] and Shockley partial dislocations on the (111)-γ interface (see also [**43**]).

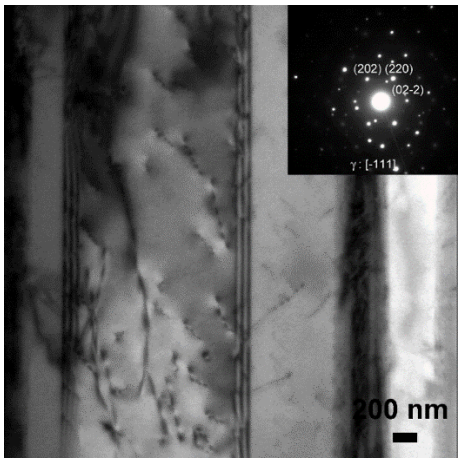

Figure 4. Dislocation loops formed upon second annealing on (111)-γ planes (Ti-46-4 annealed at 1273K).

Thus, interface reactions between the thin lamellar plates are promoted and driven by the aging temperature. This, in turns, drives the occurrence of the observed lamellar spacing widening. Quite similar results were obtained by Yamamoto and co-workers who studied an Ti-48Al-8Nb alloy aged at 1473K/3h [**45**].

The increment of the second aging treatment temperature, from 1173 to 1273K, also induced a twinning interface type evolution. That is, variant-twin (V-T), pseudo-twin (Ps-T), and perfect twin (Pe-T) were formed during aging. **Figure 5** reports representative BF-TEM and high-resolution TEM micrographs showing the peculiar morphology of these three different twin boundaries, i.e., Pe-T, Ps-T, and V-T. The 100K aging increment was found to promote a reduction of number fraction of the variant interface that halved from 1173K to 1273K, and, at the same time, a significant increment of the perfect-twin boundary number fraction. The number fraction of pseudo-twin boundaries and the number fraction of α_2 plates did not vary significantly. **Table 2** shows the statistical data of the number fraction of three different twin boundaries, that is the Pe-T, PsT, and V-T, and the number fraction of the α_2 plate boundaries, after aging at 1173 and 1273K.

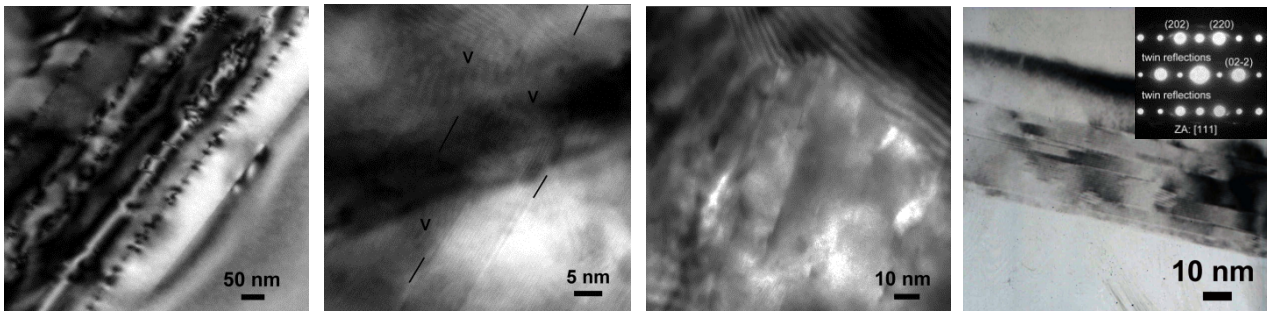

a) b) c) d)

Figure 5. BF-TEM of perfect twins (Pe-T), a), HR-TEM showing Pe-T atomic arrangements, b), pseudo-twins (Ps-T), c), and HR-TEM showing atomic arrangements of Pe-T and Ps-T with variant-twins (V-T), d). In b) lines represent the atomic alignment of Pe-T and eventually Ps-T, V stands for V-T and is placed where atomic variant dis-alignment is present in the micrograph. SAEDP recorded at the triple junction of Pe-T, Ps-t and V-T of d) is also reported in the inset. All micrographs refer to Ti-46-4 annealed at 1273K.

It resulted that the lamellar microstructure consisting mostly of the γ/γ interfaces is to some extent thermodynamically stable upon aging up to 1273K. This is also due to the significant α_2/γ boundary number fraction which is promoted by the consisted presence of the thermodynamically stable α_2 lath within the alloy microstructure. Thence, lamellae thermal stability is maintained by

aging at 1273K/1h. On the other hand, and in agreement with present results, thermal stability was shown to be maintained up to aging at 1473 K for few minutes in a Ti-48Al alloy containing the thermodynamically stable α_2 laths [**45**]. In fact, the instability of the γ lamellar microstructure is attributed to the microstructure change within lamellae during the early stage of high-temperature aging, especially when the α_2 plates are not present [**45,46**]. The present results also revealed that the twinning interface is induced to assume a perfect-twin boundary character by aging. The perfect-twin is microstructurally and crystallographically characterized by an exact mirror atomic configuration across the interface, whereas pseudo-twin has a quasi-mirror configuration with different atom configurations due to its ordered structure. The variant has the same lattice configuration but different sub-lattice configuration on both sides of the interface [**45**]. It was also observed that the curved interface were induced to line up by the aging temperature. **Figure 6** shows a typical example of the multiple curved interface with triple junction. These interfaces at the triple junction are formed by perfect-twin boundaries (right-hand side respect to the arrows), pseudo-twin boundaries (mostly not visible in the micrographs as they have a slightly different crystallographic orientation), and variant-twin boundaries (right-hand side respect to the arrows).

		1173K	1273K
	V-T	1.26 ± 0.04	0.68 ± 0.04
twin-α_2	Ps-T	0.42 ± 0.04	0.54 ± 0.03
number fraction, μm^{-1}	Pe-T	0.35 ± 0.03	1.12 ± 0.04
	α_2	0.48 ± 0.02	0.50 ± 0.03

Table 2. Line number fraction, μm^{-1}, of the four different dislocation boundaries: the three existing γ-twin boundaries (Pe-T, Ps-T, and V-T), and the number fraction of the α_2 lath boundaries as measured after aging at 1173K and 1273K.

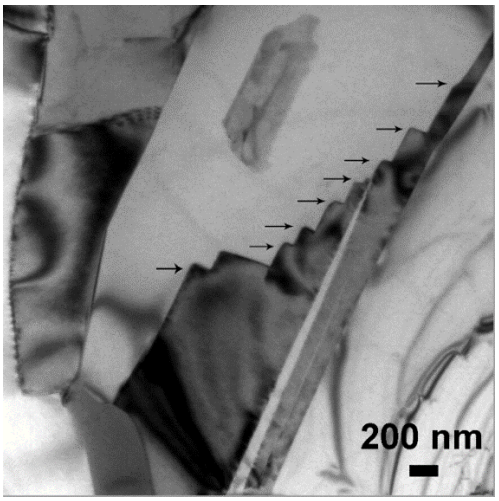

Figure 6. BF-TEM of Ti-48-4 alloy aged at 1273K showing multiple triple junctions (indicated by arrows in the figure) characterized by the formation curved variant of twin boundaries: perfect-twin (Pe-T), pseudo-twin (PsT), and the variant twin (V-T) after aging at 1273K.

3.2. Influence of aging temperature and C content on the α_2 lath width and γ-twinning character

The width of the α_2 laths decreased by rising the second annealing temperature (**Table 1**). For the Ti-46Al-4Nb alloy, without carbon additions, the α_2 lath width decrease by ~30%, from 70 to 50 nm. In the carbon-bearing alloy, the width of the α_2 laths after annealing at 1273K steadily decreased down to $L_{\alpha 2}$ = 32 ± 5 nm with 2000 wt. ppm C. The α_2 lath, $L_{\alpha 2}$, reduction process saturated as soon as the carbon content reached the lower concentration limit to initiate the formation of the *H*-Ti_2AlC phase, that is at C = 3000 wt. ppm. In this case, the α_2 lath width slightly

widened to remain constant with further C addition to the Ti-46Al-4Nb alloy up to 0.5 wt.%. On the other hand, by increasing the second annealing temperature, γ laths were induced to grow and more γ laths were induced to nucleate. This microstructure feature did contribute to some extent to the above-mentioned reduction trend of the α_2 lath width, $L_{\alpha 2}$, within the lamellar colonies (**Table 1**).

Indeed, **Table 1** reports the measured mean γ lath width, L_γ, not only for the two second aging temperatures, in the case of the bare Ti-46Al-4Nb alloy, but also for the C-bearing alloys.
The influence of the second annealing temperature on the lamellar microstructure modifications was also investigated by Sun [**47**]. He produced ultrafine fully lamellar structures in a Ti-45.3Al-2.1Cr-2Nb reporting that the average interface spacing was increased with annealing temperatures. Sun isothermally aged the alloy for few minutes (<30 min), and then the alloy was maintained close to the equilibrium state favouring coalescence of the γ lamellae. Thence, a larger average lamellae interface spacing respect to the present case was obtained in [**47**].

On the other hand, Park *et al.* [**48**] found that in Ti-46.6Al-1.4Mn-2Mo alloy the interface spacing and the lamellae widths were reduced by a factor of two with 950 wt. ppm carbon addition. They explained this behaviour by carbon segregation at α_2 grain boundaries. This interstitial element segregation was identified as the microstructure feature responsible for the stacking fault energy reduction. This in turns lead to a large number of possible nucleation sites for γ phase formation. This way, on annealing, the γ phase grows at the expense of α_2 resulting in γ lath formation in between the α_2 phase. If the number of γ nucleation sites is increased by carbon, the number of γ lath is expected to be higher and consequently the width of the α_2 laths decreased [**48**].

In addition, segregation of carbon at the ledges and kinks of α_2/γ interface hinders the thickening of the γ laths and thus leads to finer γ lamellae. Thence, the increased number of nucleation sites and the smaller lath thickening rate are the two keys factor toward the formation of a refined lamellar microstructure in Ti-46Al-4Nb intermetallic alloy with carbon addition.

As proposed by Aaronson *et al.* [**49**], transformation by terrace-ledge-kink, in which process compositional fluctuation occurs by jumping of atoms at ledges or kinks at the interphase interface, is favoured by both aging and interstitial addition to TiAl intermetallic alloys. Thence, carbon atoms segregate to the ledges and kinks at interlamellar locations. This in turns is responsible for decreasing the rate of lateral thickening of the γ lamellae. On the other hand, carbon segregation at the grain boundaries induced an increased fault frequency. This, in turns, increased the nucleation rate of the γ phase. The combined effect of increased nucleation rate and decreased thickening rate resulted in the ultrafine character of both α_2 and γ. Moreover, the thermodynamically stable α_2 plates played an important role in pinning the growth of γ grains across the lamellae, as also found in [**50**] where the existence of α_2 laths was found to be responsible for the high thermal stability of the alloy lamellar microstructure.

Figure 7 reports representative micrographs showing the role of C on the twinning width and number fraction evolution in the Ti-46-4 alloy aged at 1173 and 1273K. The TEM inspections of the alloy added with 3000 wt. ppm C showed the presence of small precipitates of *H*-Ti_2AlC phase. These were found homogeneously distributed in the γ phase, and typically formed along dislocation lines. *H* phase particles were elongated with an aspect ratio ranging 5 to 10. The typical size of the *H* particles ranged 40 to 120 nm in equivalent diameter. **Figure 8** is a representative BF-TEM showing the typical morphology and size of the *H*-Ti_2AlC phase that precipitated during second aging at 1273K in the Ti-46-4 alloy with C = 3000 wt. ppm. These particles are lens-shaped with mean equivalent diameter of 300 ± 50 μm. On the other hand, in **[51]** the Ti-48Al intermetallic alloy added with up to 3000 wt. ppm of carbon showed the presence of small *H* phase precipitates, whose mean size was of 50 nm, and homogeneously distributed in the γ phase. The *H*-Ti_2AlC lens-shaped phase has a hexagonal crystallographic structure with cell parameters a =2.977±0.003 Å and c = 13.65±0.01 Å. This is oriented as to have (0001)-*H* || (111)-γ and [11-20]-*H* || [-101]-γ, as also reported in [**52**]. The formation of this phase is driven by the low solubility of C within α_2 phase (0.12 at. %) and within γ phase (0.035 at. %) at 700-1000K [**53**].

Menand *et al.* [**53**] showed that, in two-phase Ti intermetallic alloys, the γ phase saturates by interstitial content of ~250 at. ppm, the excess interstitials forming solid solution within the α_2 phase. Precipitation occurs as soon as also the α_2 phase saturates by increasing the amount of the interstitial elements. With this respect, the solubility limit of C in α_2 is evaluated at ~3000 wt. ppm (~9600 at. ppm) [**53**].
The statistical evaluation of interlamellar spacing of both γ/α_2 and γ/γ and the related lamellae width showed a clear reduction with alloy carbon contents. A well-defined threshold lower limit was detected and this was identified as C ≅ 3000 wt. ppm.

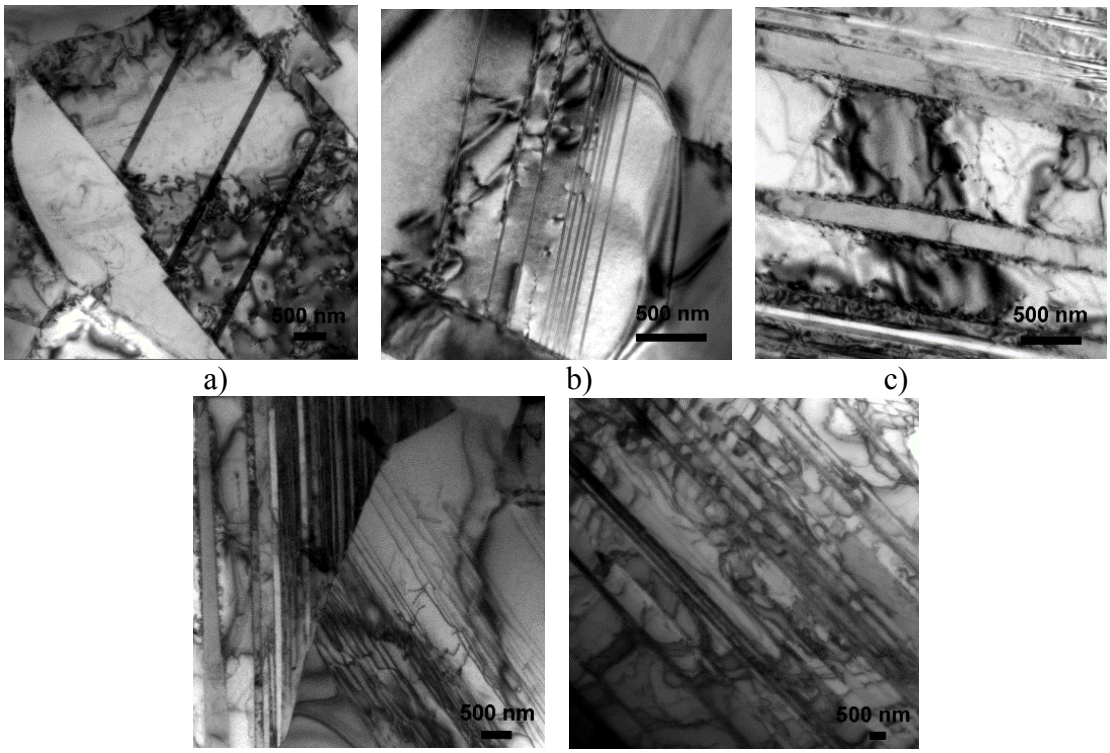

Figure 7. Representative BF-TEM showing the role of C on the twinning width and number fraction evolution; Ti-46-4 with C = 500 wt. ppm, a), C = 1000 wt. ppm, b), C = 2000 wt. ppm, c), C = 3000 wt. ppm, d), C = 5000 wt. ppm, e). All micrographs refer to second aging at 1273K.

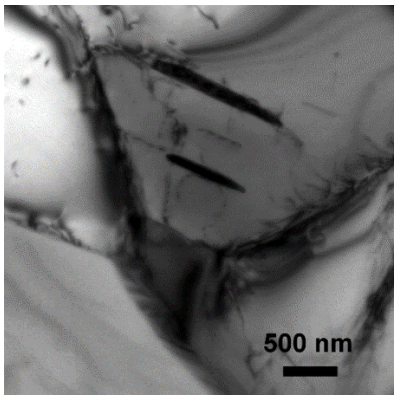

Figure 8. BF-TEM of *H*-Ti_2AlC phase (Ti-46-4 aged at 1273K).

The present results appeared to be in good agreement with previous findings reported by Perdrix *et al.* [**51**] with a similar intermetallic alloy. In their work, they found that carbon contents from 20 to

1000 wt. ppm induced the α_2 volume fraction, $F_V(\alpha_2)$, to increase and the interlamellar spacing, *IS*, that is, the mean spacing between two consecutive α_2 lamellae to decrease. Perdrix *et al.* [**51**] identified a carbon threshold limit at ~1000 wt. ppm in a Ti-48Al alloy. These trends are similar to those observed in alloys with oxygen [**54**] or nitrogen additions [**55**]. Yet, the transition observed at about 1000 wt. ppm for C is higher for N (3000 wt. ppm) and still higher for O (>6000 wt. ppm) [**48,54-56**]. In the present case, the threshold concentration limit of carbon was found to consisstency higher (C ≅ 3000 wt. ppm) and this is likely to bedue to the presence of Nb in the intermetallic alloy and to the second aging temperature (1273K) to which the alloy was subjected. In fact, all the interstitial elements do form a similar *H* phase, when they are added to the intermetallic TiAl alloy above a certain upper cut-off concentration limit. This is different from element to element, but the formation of the *H* phase is anyway favoured. Then, the same crystallographic configuration and symmetry, with a *H*-Ti_2AlX stoichiometry, where *X* is the specific interstitial element added to the alloy is formed in these interstitial elements added TiAl-based intermetallic alloys.

With this respect, Perdrix *et al.* [**55**] reported the formation of *H*-Ti_2AlN within the γ-phase in an alloy with high nitrogen content. These small lens-shaped precipitation particles were homogeneously distributed within the γ-phase and heterogeneously on dislocations, with particle mean size of 50 nm. In the N-bearing TiAl alloy microhardness was reported to increase linearly for N amount up to 3000 wt. ppm. For N contents above 3000 wt. % the hardness remained unchanged irrespectively of the N content, as the excess of N started to form *H*-Ti_2AlN particles [**55**].

The here obtained results seem to indicate that carbon, as long as this interstitial element remains in solid solution, promoted α_2 phase stability by increasing $F_V(\alpha_2)$ and decreasing *IS*. On the other hand, whenever carbon solid solution saturates within the α_2 phase, $F_V(\alpha_2)$, and *IS* were reported to remain constant.

	Ti-46-4	Ti-46-4+ 500 wt. ppm C	Ti-46-4+ 1000 wt. ppm C	Ti-46-4+ 2000 wt. ppm C	Ti-46-4+ 3000 wt. ppm C	Ti-46-4+ 5000 wt. ppm C
V-T	0.24 ± 4%	0.22 ± 4%	0.20 ± 4%	0.17 ± 4%	0.12 ± 3%	0.05 ± 3%
Ps-T	0.19 ± 8%	0.16 ± 8%	0.15 ± 8%	0.12 ± 8%	0.09 ± 5%	0.03 ± 3%
Pe-T	0.39 ± 8%	0.42 ± 6%	0.42 ± 5%	0.45 ± 4%	0.49 ± 3%	0.62 ± 3%
α_2	0.18 ± 4%	0.20 ± 4%	0.23 ± 4%	0.26 ± 4%	0.30 ± 3%	0.30 ± 3%

Table 3. Normalized number fraction of γ-twin boundaries: Pe-T, Ps-T, and V-T, and α_2 lath boundaries as function of C addition to the Ti-46-4 alloy, after second aging at 1273K.

3.3. Correlation between hardness and microstructure

Microhardness, HV_5, seems to follow α_2 volume fraction and the lamellae width reduction trend very closely. With this respect, **Figure 9** shows the $F_V(\alpha_2)$ and HV_5 as a function of the C wt. content. The carbon-free alloys aged at 1173K had α_2 lath volume fraction $F_V(\alpha_2)$ = 39% and a hardness of 440 HV_5. The hardness and $F_V(\alpha_2)$ tended to increase by rising the second aging temperature from 1173 to 1273K. This was also observed in a similar studies carried out on a Ti-45Al-7.5Nb alloy by Cha *et al.* [**57**]. As for the influence of carbon, **Figure 9** clearly shows that both $F_V(\alpha_2)$ and HV_5 increased with carbon content from 500 to 5000 wt. ppm, as long as α_2 phase is enriched with carbon as solid solution element. Then the two parameters remain constant as soon as the α_2 phase saturated with carbon and *H*-Ti_2AlC phase precipitates in the γ phase. However, besides this α_2 volume fraction effect, the microhardness of the lamellar alloy is also dependent on the α_2 phase volume fraction. On the contrary, precipitation of the *H*-Ti_2AlC phase does not affect to a significant extent the microhardness. A similar trend of both $F_V(\alpha_2)$ and *HV* was also reported by Perdrix *et al.* in a Ti-48Al intermetallic alloy [**51**].

Moreover, Cam *et al.* [**58**], showed that all interstitial elements stabilize the α_2 phase (that is, C as well as N and O). Both Cam *et al.* [**58**] and Park *et al.* [**48**] reported that the lamellae colony size

was not significantly affected by the addition of less than 3000 at. ppm of C (corresponding to 950 wt. ppm), although γ and α_2 lamella mean widths decreased markedly.

Thence, carbon in solid solution increased the microhardness indirectly by increasing $F_V(\alpha_2)$, and directly by increasing the α_2 microhardness contribution given by increasing the C amount in solid solution. The latter effect was more effective than the former one. Then, as soon as the α_2 phase saturates with carbon, microhardness and $F_V(\alpha_2)$ no longer varied. On the other hand, low-width α_2 laths resulted in a higher hardness.

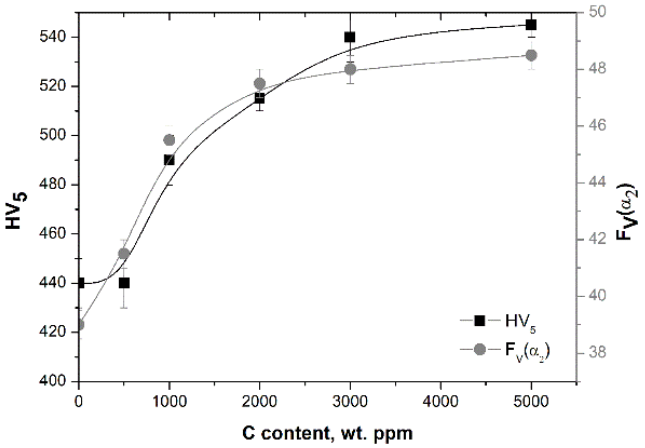

Figure 9. H and $F_V(\alpha_2)$ vs. C (wt. ppm) content.

According to the Hall–Petch (HP) mechanism, not just high-angle boundaries (grain boundaries) but also all kind of interfaces, *i.e.* in the present case both γ/α_2 and γ/γ, and twinning within the γ phase, act as obstacles for the gliding dislocations. Thus, the HP-dependent alloy mechanical properties are significantly improved whenever the interface density is high, as well as they are greatly improved whenever the grained boundary density is high (that is upon grain size reduction). Similarly, a dislocation strengthening mechanism is also acting in the alloy. The existing dislocations within the lamellae strengthen the alloy by an Orowan-type dislocation mechanism. Consequently, alloy hardness is directly related to the combined Hall-Petch and Orowan strengthening mechanisms primarily through lamellar spacing refinement. Indeed, this issue was already discussed and applied by Takeyama *et al.* [**59**] in a binary Ti-48Al, and by Dehm *et al.* [**60**] in a more complex γ-TiAl based alloy. They both reported quite a similar hardness response to the alloy microstructure lamellae evolution driven by the different applied experimental conditions.

Thence, in order to account to the alloy hardness response driven by the amount of the added carbon content and by the second aging temperature, the two terms, Hall-Petch and Orowan strengthening, are here discussed. The Orowan relationship is expressed as $HV \cong MGb/\lambda$, where M = 2.8 is the Taylor factor, G is the alloy shear modulus, b the Burgers vector, and λ the mean lamellae width of both γ and α_2. Since, the present alloy is composed by a mixture of two interconnected phases (γ and α_2), a composite-like hardness relationship is here proposed, Eq. (1a):

$$\frac{1}{HV} \cong \frac{f_\gamma}{HV_\gamma} + \frac{f_{\alpha 2}}{HV_{\alpha 2}} \qquad (1a)$$

where f_γ and $f_{\alpha 2}$ are the volume fraction of the γ and α_2 phases, HV_γ and $HV_{\alpha 2}$ are the hardness contributions of each phase, γ and α_2.

Substituting the Orowan relation for each phase, Eq (1a), can be rewritten as, Eq. (1b):

$$\frac{1}{HV} \cong \frac{1}{M}\left[\frac{f_\gamma \lambda\gamma}{G_\gamma b_\gamma} + \frac{f_{\alpha 2}\lambda_{\alpha 2}}{G_{\alpha 2} b_{\alpha 2}}\right] \qquad (1b)$$

In the present study the shear modules were set to $G_\gamma = G_{\alpha 2} = 70$ GPa, as determined from a theoretical study by Yoo *et al.* in a similar γ/α_2 binary Ti-49Al alloy [**61**]. On the other hand, the tendency of slight increase of the Burgers vector by the C solute concentration within the two constituting phases is quite slugghish and the value of b = 0.28 nm of the Ti46Al-4Nb can be considered essentially constant with increasing carbon content. That is, Eq. (1b) can be rewritten as, Eq. (1c):

$$\frac{1}{HV} \cong \frac{f_\gamma \lambda_\gamma + f_{\alpha 2} \lambda_{\alpha 2}}{MGb} \rightarrow HV \cong \frac{MGb}{f_\gamma \lambda_\gamma + f_{\alpha 2} \lambda_{\alpha 2}} \quad (1c)$$

The variation of both γ laths and α_2 lamellae width with alloy carbon content is reported in **Table 4**. The corresponding alloy strength and the obtained discrepancy with the experimental values coming form the direct hardness measurements is also reported.

	Ti-46-4	Ti-46-4+ 500 wt. ppm C	Ti-46-4+ 1000 wt. ppm C	Ti-46-4+ 2000 wt. ppm C	Ti-46-4+ 3000 wt. ppm C	Ti-46-4+ 5000 wt. ppm C
λ_γ, nm	50	50	42	40	38	38
$\lambda_{\alpha 2}$, nm	25	25	25	25	22	22
alloy strength from Eq.(1c), MPa	1360	1385	1600	1670	1810	1815
alloy strength from measured *HV*, MPa	1450	1450	1660	1750	1870	1870
discrepancy, %	6	4	4	5	3	3

Table 4. γ twinning width, λ_γ, and α_2 lamellae lath width, $\lambda_{\alpha 2}$, as function of C addition to the Ti-46-4 alloy, after second aging at 1273K.

The present results clearly show that the hardness increased by reducing the lateral size of the twinning in the γ phase, which actually hinders dislocation sliding. Thence, in ultrafine $\gamma + \alpha_2$ lamellar alloy the hardness resulted to depend on both the α_2 volume fraction and the $\gamma + \alpha_2$ lamellar width. It should be noted that whenever both the γ and α_2 lath widths are in the nano-scale region, the relative volume of the two phases becomes an important parameter. Similarly, in [**57**] hardness increased with both second aging temperature and carbon addition, that is, by reducing the lamellar spacing and γ, α_2 lath widths.

Perdrix *et al.* [**51**] investigated sub-micrometer- and micrometer-size lamellar microstructures in Ti-48Al alloys with different carbon additions and reported hardness increase with carbon content up to 1.8 at. %. They found α_2 lamellae size ~500 nm irrespective of the carbon content. The α_2 volume fraction increased significantly up to the upper limit of carbon content (0.9 at. %), where precipitation of the *H* phase started. Perdrix *et al.* [**51**] seemed to confirm that the hardness is directly correlated to both the α_2 phase amount within the two-phase alloy, and to the solid-solution amount of the interstitial element present within the two-phase microstructure.

4. Conclusions

The evolution of γ/γ and γ/α_2 interfaces with carbon addition to a Ti–46Al–4Nb intermetallic alloy was characterized by electron microscopy techniques. The hardness influence on the γ twins and α_2 lamellae widths was also determined. In particular the following major findings can be outlined:

i. Progressive amounts of carbon, from 500 to 5000 wt. ppm, have been added to the Ti-46Al4Nb intermetallic alloy in which a fully lamellar microstructure was obtained by aging at 1273K.
ii. Carbide precipitates of *H*-Ti_2AlC phase appeared to form as soon carbon concentrations in the alloy reached 3000 wt. ppm. The occurrence of *H*-Ti_2AlC phase did not change significantly the lamellar spacing.
iii. Carbon in solid solution increased the α_2 volume fraction and decreases the mean distance between α_2 lamellae upon aging at 1273K.
iv. The carbon content greatly promoted a progressive modification of the different two-phase structure boundaries. The Ti-46Al-4Nb was characterized by an almost equal number fraction presence of variant-twinning, pseudo-twinning, perfect-twin and α_2 lath boundaries Increasing carbon content in the alloy induced a progressive promotion of perfect-twin and α_2 lath boundaries at the expense of the other two types of twin boundaries, variant-twin and pseudo-twin. The formation of the *H*-phase did not constrast this tendency, although it seemed to induce a process saturation.
v. Microhardness increased by solute carbon content in the alloy to reach a saturation limit at C ≅ 3000 wt. ppm, that is as soon as the *H*-phase started to form at the expense of the solute concentration. Corresppndingly, the α_2 lath volume fraction followed a similar trend with carbon content and it also saturated whenever carbon reached the alloy solute limit concentration to inititate the precipitation of the *H*-phase out of the excess of solute content. That is, the alloy hardness appeared to strongly depend on the α_2 lamellae width and volume fraction, this,in turns, appeared to be influenced by the second aging temperature and the chemical composition (namely solute carbon content).

Acknowledgments

The EU-funded COST Action CA15102 - Solutions for Critical Raw Materials under Extreme Conditions (CRM-EXTREME), website: https://www.cost.eu/actions/CA15102, is acknowledged for the material supply.

References

[1] Y.W. Kim, Ordered intermetallic alloys, part III: Gamma titanium aluminides, JOM 46 (1994) 30-39.
[2] Y. Yamabe, M. Kikuchi, Report of the 123rd Committee on Heat-Resisting Materials and Alloys, Japan Society for the Promotion of Science, 31 (1990) 179-195.
[3] T. Kawabata, T.T. Abumiya, T. Kanai, O. Izumi, Mechanical properties and dislocation structures of TiAl single crystals deformed at 4.2–293 K, Acta metall. mater. 38 (1990) 1381-1393.
[4] G. Hug, A. Loiseau and A. Lasalmonie, Nature and dissociation of the dislocations in TiAl deformed at room temperature, Phil. Mag. A 54 (1986) 47-65.
[5] J.T. Kandra, E.W. Lee, Temperature and microstructural dependence of the deformation of a high Nb Ti-Al alloy, Metals Mater. Trans. A 25 (1994) 1667-1679.
[6] M.A. Morris, Dislocation configurations in two-phase Ti[sbnd]Al alloys III. Mechanisms producing anomalous flow stress dependence on temperature, Phil. Mag. A 69 (1994) 129-138.
[7] H. A. Lipsitt, D. Shechtman and R. E. Schafrik, The deformation and fracture of TiAl at elevated temperatures, Metall. Trans. A 6 (1975) 1991-1996.
[8] S. A. Court, P. A. Lofvander, M. H. Loretto and H. L. Fraser, The influence of temperature and alloying additions on the mechanisms of plastic deformation of Ti_3Al, Phil. Msg. A 61 (1990) 109-139.

[9] M. Tanimura, Y. Inoue, Y. Koyama, M. Kikuchi, Change in Microstructure during Aging at 1273K in Ti-40at.%Al alloy, Mater. Trans JIM 37 (1996) 1190-1196.
[10] Yamabe Y, Takeyama M, Kikuchi, Microstructure evolution through solid-solid phase transformations in gamma titanium aluminides, In: Kim YW, Wagner R, Yamaguchi H, editors. Gamma titanium aluminides. Annual meeting and exhibition of the Minerals, Metals and Materials Society (TMS), Las Vegas, NV (United States), 12-16 Feb 1995, TMS, (1995) 111-118.
[11] Y.W. Kim, Effects of microstructure on the deformation and fracture of γ-TiAl alloys, Mater. Sci. Eng. A 192-193 (1995) 519-533.
[12] W. Schillinger, H. Clemens, G. Dehm, A. Bartels, Microstructural stability and creep behavior of a lamellar γ-TiAl based alloy with extremely fine lamellar spacing, Intermetallics 10 (2002) 459-466.
[13] P.J. Maziasz, C.T. Liu, Development of ultrafine lamellar structures in two-phase γ-TiAl alloys, Metall. Mater. Trans. A 29 (1998) 105-117.
[14] H. Zhu, J. Matsuda, K. Maruyama, Influence of heating rate in α + γ dual phase field on lamellar morphology and creep property of fully lamellar Ti-48Al alloy, Mater. Sci. Eng. A 397 (2005) 58-64.
[15] Y.Q. Sun, Surface relief and the displacive transformation to the lamellar microstructure in TiAl, Phil. Mag.Lett. 78 (1998) 297-305.
[16] Y.Q. Sun, Nanometer-scale, fully lamellar microstructure in an aged TiAl-based alloy, Metall. Mater. Trans. A 29 (1998) 2679-2685.
[17] H. Clemens, A. Bartels, S. Bystrzanowski, H. Chladil, H. Leitner, G. Dehm G, R. Gerling, F.P. Schimansky, Grain refinement in γ-TiAl-based alloys by solid state phase transformations, Intermetallics 14 (2006) 1380-1385.
[18] W. Lefebvre, A. Menand, A. Loiseau, Influence of oxygen on phase transformations in a Ti-48 At. pct Al alloy, Metall. Mater. Trans. A 34 (2003) 2067-2075.
[19] Y.W. Kim, Microstructural evolution and mechanical properties of a forged gamma titanium aluminide alloy, Acta Metall. Mater. 40 (1992) 1121-1134.
[20] R.V. Ramanujan, P.J. Maziasz, The mechanism of formation of a fine duplex microstructure in Ti-48Al-2Mn-2Nb alloys, Metall. Mater. Trans. A 27 (1996) 1661-1673.
[21] C.T. Liu, J.H. Schneibel, P.J. Maziasz, J.L. Wright, D.S. Easton, Tensile properties and fracture toughness of TiAl alloys with controlled microstructures, Intermetallics 4 (1996) 429-440.
[22] H. Zhu, J. Matsuda, K. Maruyama, Microstructural refinement mechanism by controlling heating process in multiphase materials with particular reference to γ-TiAl, Appl. Phys. Lett. 88 (2006) 131908.
[23] W.H. Tian, M. Nemoto, Effect of carbon addition on the microstructures and mechanical properties of y-TiAl alloys, Intermetallics 5 (1997) 237-244.
[24] S.J. Yang, S.W. Nam, Investigation of α2/γ phase transformation mechanism under the interaction of dislocation with lamellar interface in primary creep of lamellar TiAl alloys, Mater. Sci. Eng. A 329-331 (2002) 898-905.
[25] G. Cao, L. Fu, J. Lin, Y. Zhang, C. Chen, The relationships of microstructure and properties of a fully lamellar TiAl alloy, Intermetallics 8 (2000) 647-653.
[26] M. Perez-Bravo, I. Madariaga, K. Ostolaza, M. Tello, Microstructural refinement of a TiAl alloy by a two step heat treatment, Scripta Mater. 53 (2005) 1141-1146.
[27] M. Beschliesser, A. Chatterjee, A. Lorich, W. Knabl, H. Kestler, G. Dehm, H. Clems, Designed fully lamellar microstructures in a γ-TiAl based alloy: adjustment and microstructural changes upon long-term isothermal exposure at 700 and 800 °C, Mater. Sci. Eng. A 329-311 (2002) 124-129.
[28] D.S. Shih, R.A. Amato, interface reaction between Gamma-TiAl alloys and reinforcement, Scripta Metall. Mater. 24 (1990) 2053-2058.
[29] Y.W. Kim, D.M. Dimiduk, Progress in the understanding of gamma titanium aluminides, JOM 43 (1991) 40-47.

[30] S. Djanarthany, C. Servant, R. Penelle, Influence of an increasing content of molybdenum on phase transformations of Ti-Al-Mo aluminides - relation with mechanical properties, Mater. Sci. Eng. A 152 (1992) 48-53.
[31] S.G. Pyo, Y.W. Chang, N.J. Kim, Microstructure and mechanical properties of duplex TiAl alloys containing Mn, Met. Mater. 1 (1995) 107-115.
[32] P.D. Crofts, P. Bowen, I.P. Jones, The effect of lamella thickness on the creep behavior of Ti-48Al-2Nb-2Mn, Scripta Metall. Mater. 35 (1996) 1391-1396.
[33] S.G. Pyo, S.M. Choi, M.S. Yoo, J.K. Oh, S.K. Whang, N.J. Kim, Nucleation and growth of α phase in hot extruded Ti-46.6Al-2Mo-1.4Mn intermetallic alloy produced by hot extrusion of elemental powders, Mater. Sci. Eng. A 374 (2004) 160-169.
[34] A. Denquin, S. Naka, Phase transformation mechanisms involved in two-phase TiAl-based alloys-I. Lambellar structure formation, Acta Metall. 44 (1996) 343-352.
[35] A. Denquin, S. Naka, Phase transformation mechanisms involved in two-phase TiAl-based alloys-II. Discontinuous coarsening and massive-type transformation, Acta Metall. 44 (1996) 353-365.
[36] K.S. Chan, J. Onstott, K.S. Kumar, The fracture resistance of a binary TiAl alloy, Met. Trans. A 31 (2000) 71-80.
[37] S. Zghal, S. Naka, A. Couret, A quantitative TEM analysis of the lamellar microstructure in TiAl based alloys, Acta Metall. 45 (1997) 3005-3015.
[38] W.J. Zhang, L. Francesconi, E. Evangelista, G.L. Chen, Characterization of widmanstätten laths and interlocking boundaries in fully-lamellar TiAl-base alloy, Scripta Mater. 37 (1997) 627-633.
[39] M. Yamaguchi, Y. Umakoshi, The deformation behaviour of intermetallic superlattice compounds, Progr. Mater. Sci. 34 (1990) 1-148.
[40] F. Appel, M. Oehring, J.D.H. Paul, C. Klinkenberg, T. Carneiro, Physical aspects of hot-working gamma-based titanium aluminides, Intermetallics 12 (2004) 791-802.
[41] Y.Q. Sun, Nanometer-Scale, Fully Lamellar Microstructure in an Aged TiAl-Based Alloy, Metall. Mater. Trans. A 29 (1998) 2679-2685.
[42] B.K. Kad, P.M. Hazzledine, Shear boundaries in lamellar TiAl, Phil. Mag. Lett. 66 (1992) 133-139.
[43] F. Appel, R. Wagner, Microstructure and deformation of two-phase γ-titanium aluminides, Mater. Sci. Eng. R 22 (1998) 187-268.
[44] H. Inui, A. Nakamura, M.H. Oh, M. Yamaguchi, High-resolution electron microscope study of lamellar boundaries in Ti-rich TiAl polysynthetically twinned crystals, Ultramicroscopy 39 (1991) 268-278.
[45] Y. Yamamoto, M. Takeyama, T. Matsuo, Stability of lamellar microstructure consisting of γ/γ interfaces in Ti–48Al–8Nb single crystal at elevated temperatures, Mater. Sci. Eng. A 329-331 (2002) 631-636.
[46] H. Inui, M.H. Oh, A. Nakamura, M. Yamaguchi, Ordered domains in tial coexisting with ti3al in the lamellar structure of ti-rich tial compounds, Phil. Mag. A 66 (1992) 539-555.
[47] Y.Q. Sun, Nanometer-scale, fully lamellar microstructure in an aged TiAl-based alloy, Metall. Mater. Trans. A 29 (1998) 2679-2685.
[48] H.S. Park, S.W. Nam, N.J. Kim, S.K. Hwang, Refinement of the lamellar structure in TiAl-based intermetallic compound by addition of carbon, Scripta Mater. 41 (1999) 1197-1203.
[49] H. I. Aaronson, Atomic mechanisms of diffusional nucleation and growth and comparisons with their counterparts in shear transformations, Metall. Trans. A 24 (1993) 241-276.
[50] D. Blavette, P. Duval, L. Letellier, M. Guttmann, Atomic-scale APFIM and TEM investigation of grain boundary microchemistry in Astroloy nickel base superalloys, Acta Mater. 44 (1996) 4995-5005.

[51] F. Perdrix, M.-F. Trichet, J.-L. Bonnentien, M. Cornet, J. Bigot, Relationships between interstitial content, microstructure and mechanical properties in fully lamellar Ti-48Al alloys, with special reference to carbon, Intermetallics 9 (2001) 807-815.
[52] W. H. Tia, M. Nemoto, Effect of carbon addition on the microstructures and mechanical properties of y-TiAl alloys, Intermetallics 5 (1997) 237-244.
[53] A. Menand, A. Huguet, A. Nérac-Partaix, Interstitial solubility in γ and α_2 phases of TiAl-based alloys, Acta Mater. 44 (1996) 4729-4737.
[54] H. Zhong, Y. Yang, J. Li, J. Wang, T. Zhang, S. Li, J. Zhang, Influence of oxygen on microstructure and phase transformation in high Nb containing TiAl alloys, Mater. Letters 83 (2012) 198-201.
[55] F. Perdrix, M.-F. Trichet, J.-L. Bonnentien, M. Cornet, J. Bigot, Influence of nitrogen on the microstructure and mechanical properties of Ti-48Al alloy, Intermetallics 19 (2001) 147-155.
[56] H.S. Cho, S.W. Nam, J.H. Yun, D.M. Wee, Effect of 1 at.% nitrogen addition on the creep resistance of two phase TiAl alloy, Mater. Sci. Eng. A 262 (1999) 129-136.
[57] L. Cha, C. Scheu, H. Clemens, H.F. Chladil, G. Dehmb, R. Gerling, A. Bartels, Nanometer-scaled lamellar microstructures in Ti-45Al-7.5Nb-(0; 0.5)C alloys and their influence on hardness, Intermetallics 16 (2008) 868-875.
[58] G. Cam, H.M. Flower, D.R.F. West, The alloying of titanium aluminides with carbon. High-Temperature Ordered Intermetallic Alloys III MRS Proceedings, 133 (1988) 663-669.
[59] T. Kumagai, E. Abe, M. Takeyama, M. Nakamura, Microstructural evolution of massively transformed γ-TiAl during isothermal aging, Scripta Mater 36 (1997) 523-529.
[60] G. Dehm, C. Motz, C. Scheu, H. Clemens, P. Mayrhofer, C. Mitterer, Mechanical size-effects in miniaturized and bulk materials, Adv. Eng. Mater. 8-11 (2006) 1033-1045.
[61] M.H. Yoo, J. Zou, C.L. Fu, Mechanistic modeling of deformation and fracture behavior in TiAl and Ti_3Al, Mater. Sci. Eng. A 192-193 (1995) 14-23.

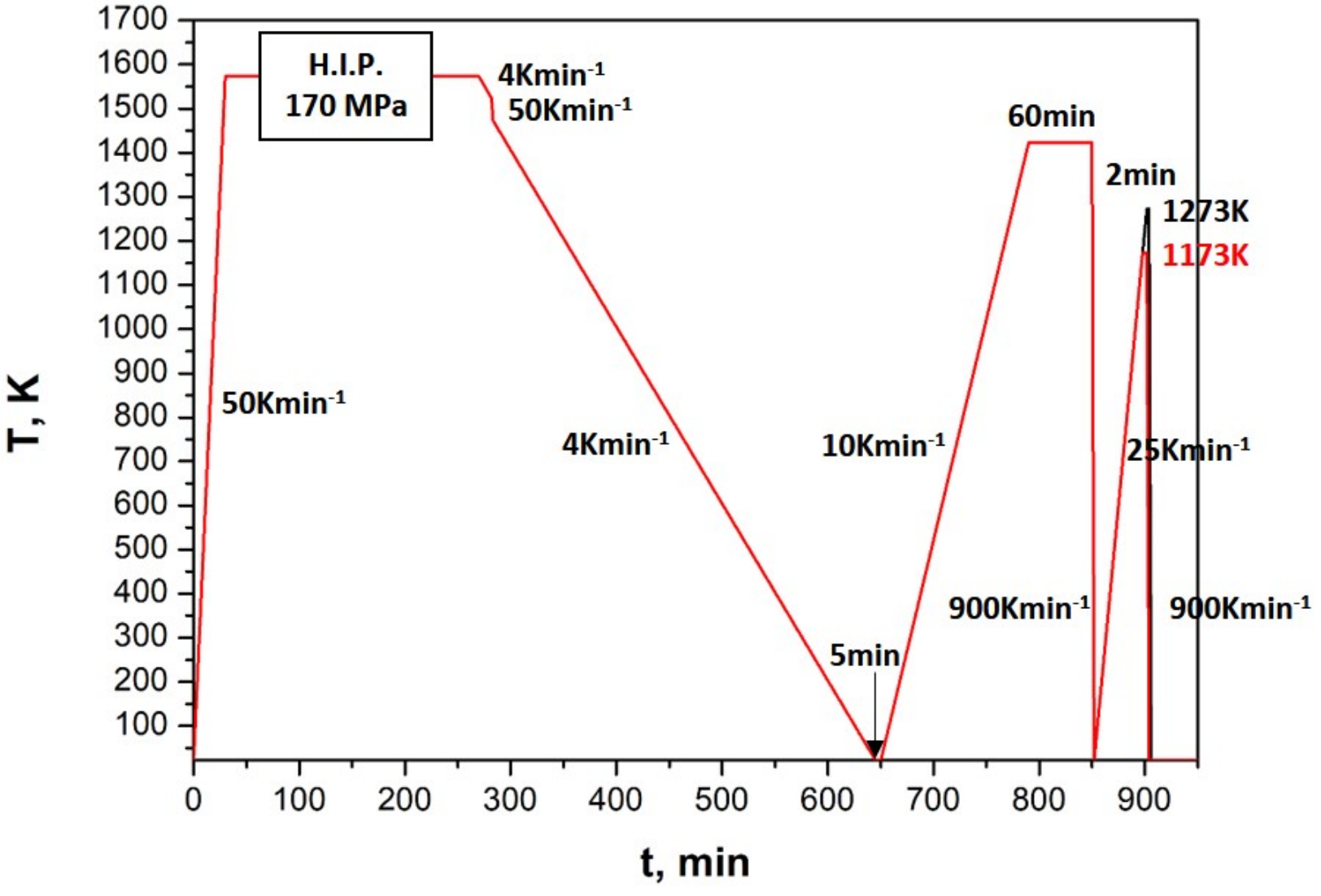
T, K
t, min
H.I.P.
170 MPa
50Kmin-1
4Kmin-1
50Kmin-1
4Kmin-1
10Kmin-1
60min
2min
1273K
1173K
25Kmin-1
900Kmin-1
900Kmin-1
5min
1700
1600
1500
1400
1300
1200
1100
1000
900
800
700
600
500
400
300
200
100
0
100
200
300
400
500
600
700
800
900

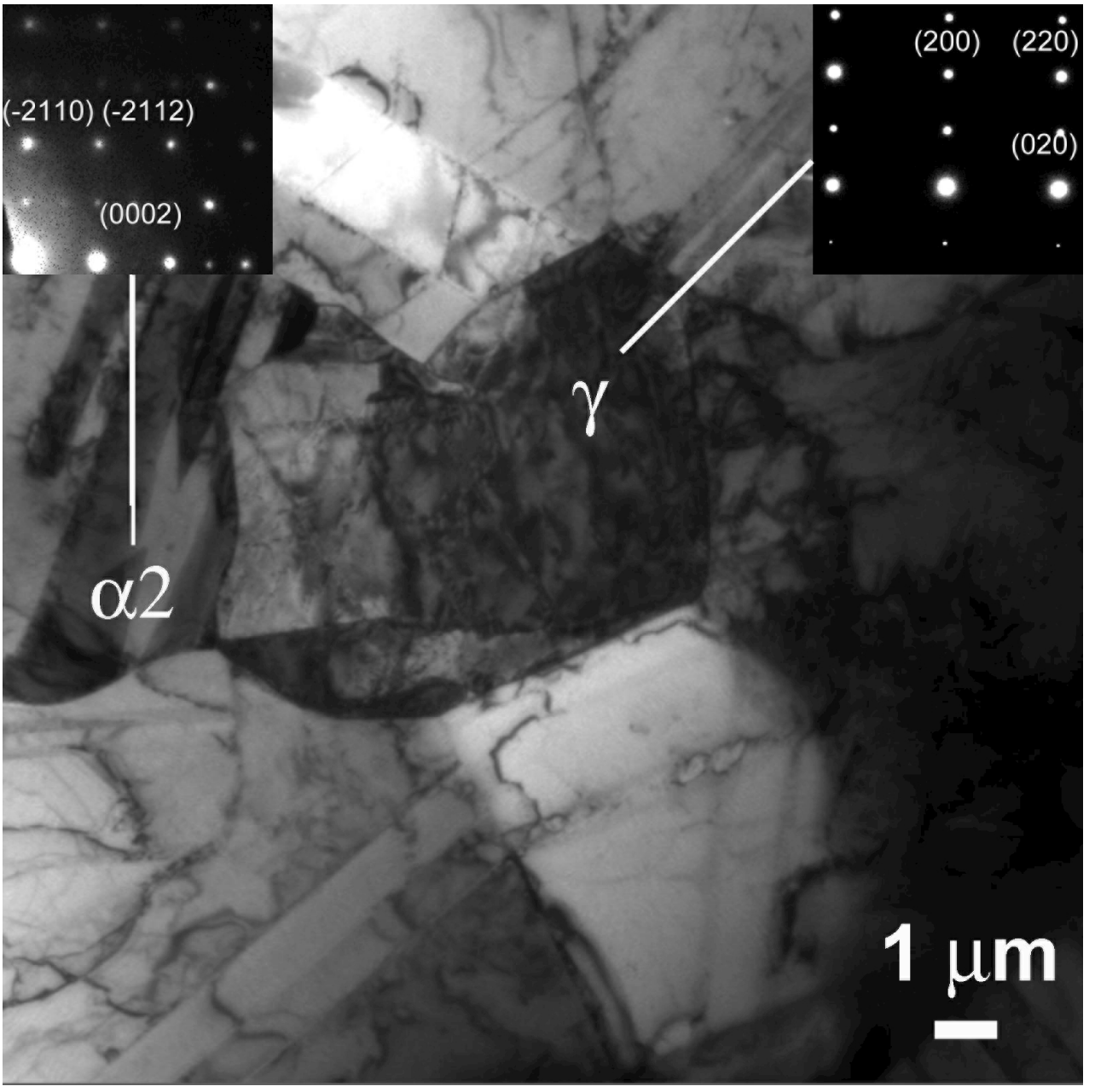
(-2110) (-2112)
(0002)
(200) (220)
(020)
γ
α2
1 μm

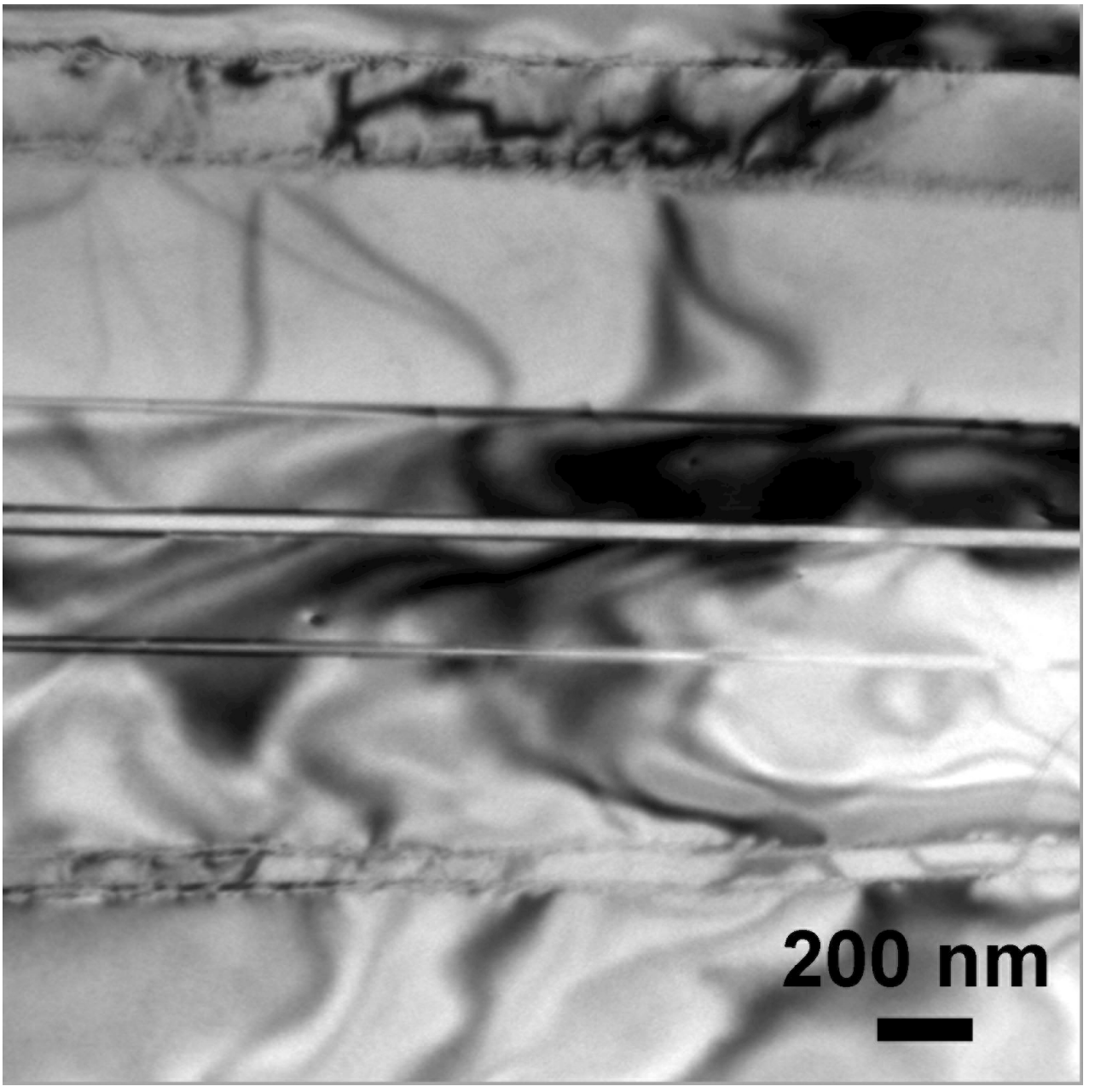
200 nm

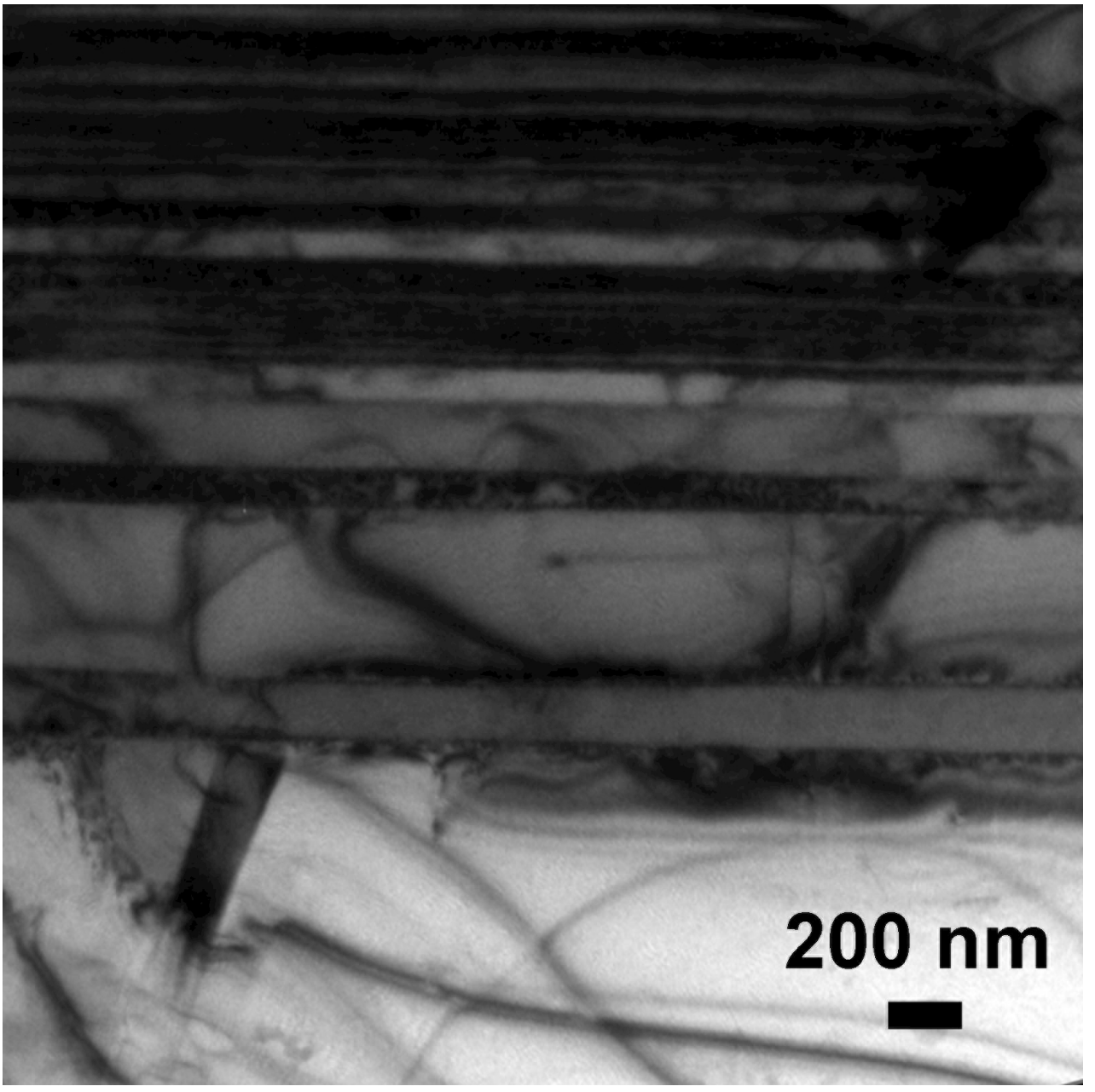
200 nm

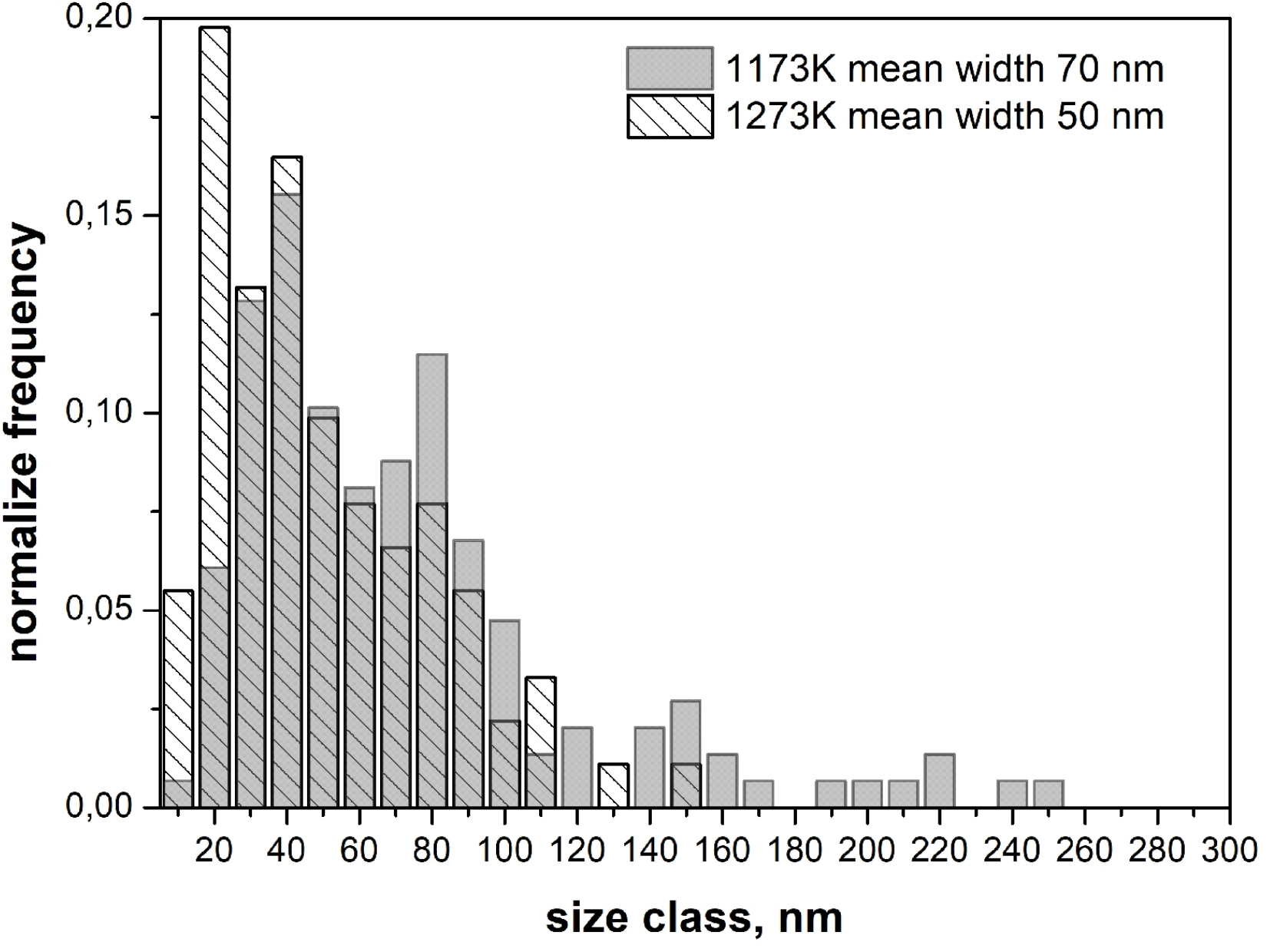
1173K mean width 70 nm
1273K mean width 50 nm
normalize frequency
0,20
0,15
0,10
0,05
0,00
20
40
60
80
100
120
140
160
180
200
220
240
260
280
300
size class, nm

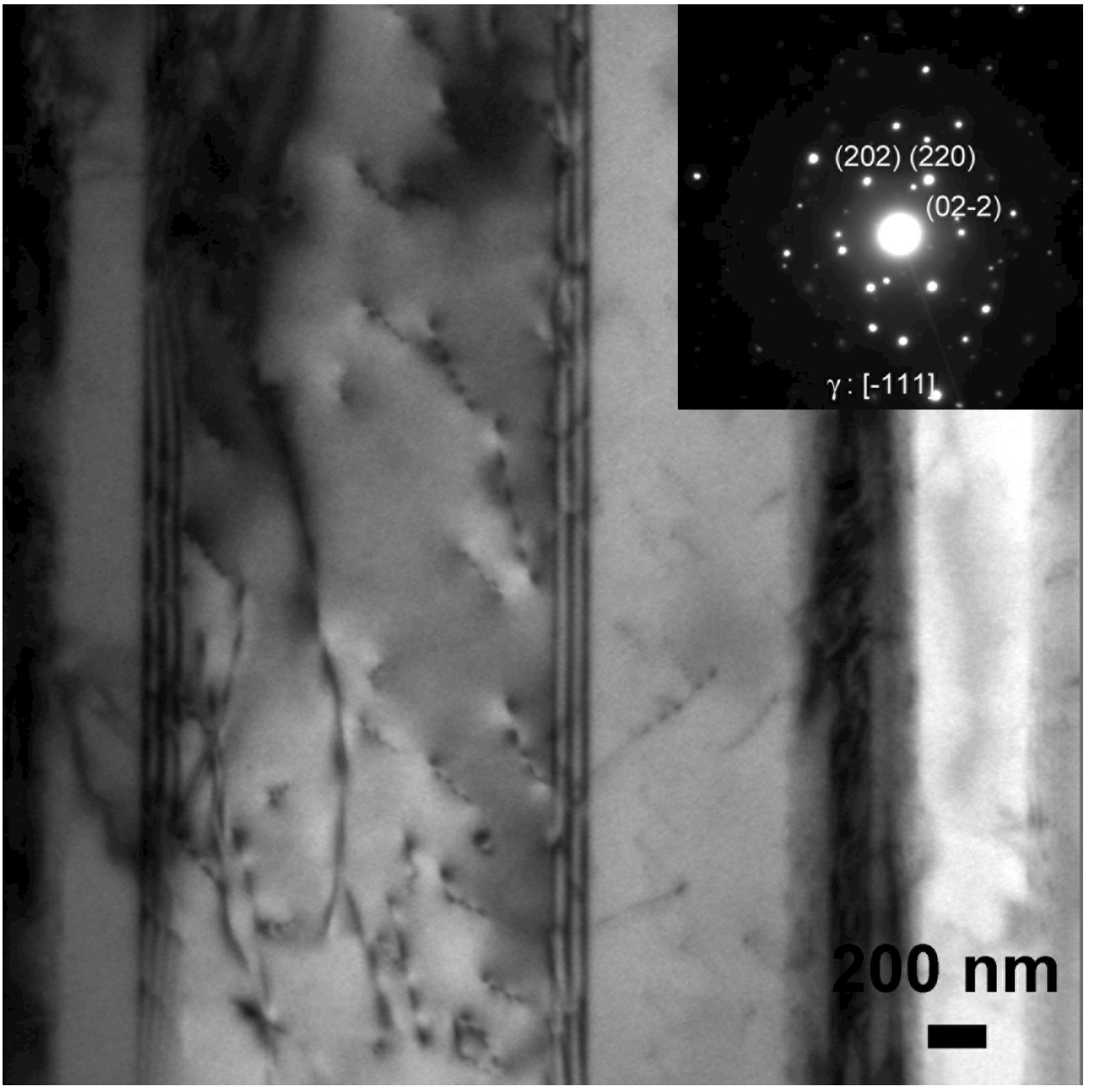
(202) (220)
(02-2)
γ : [-111]
200 nm

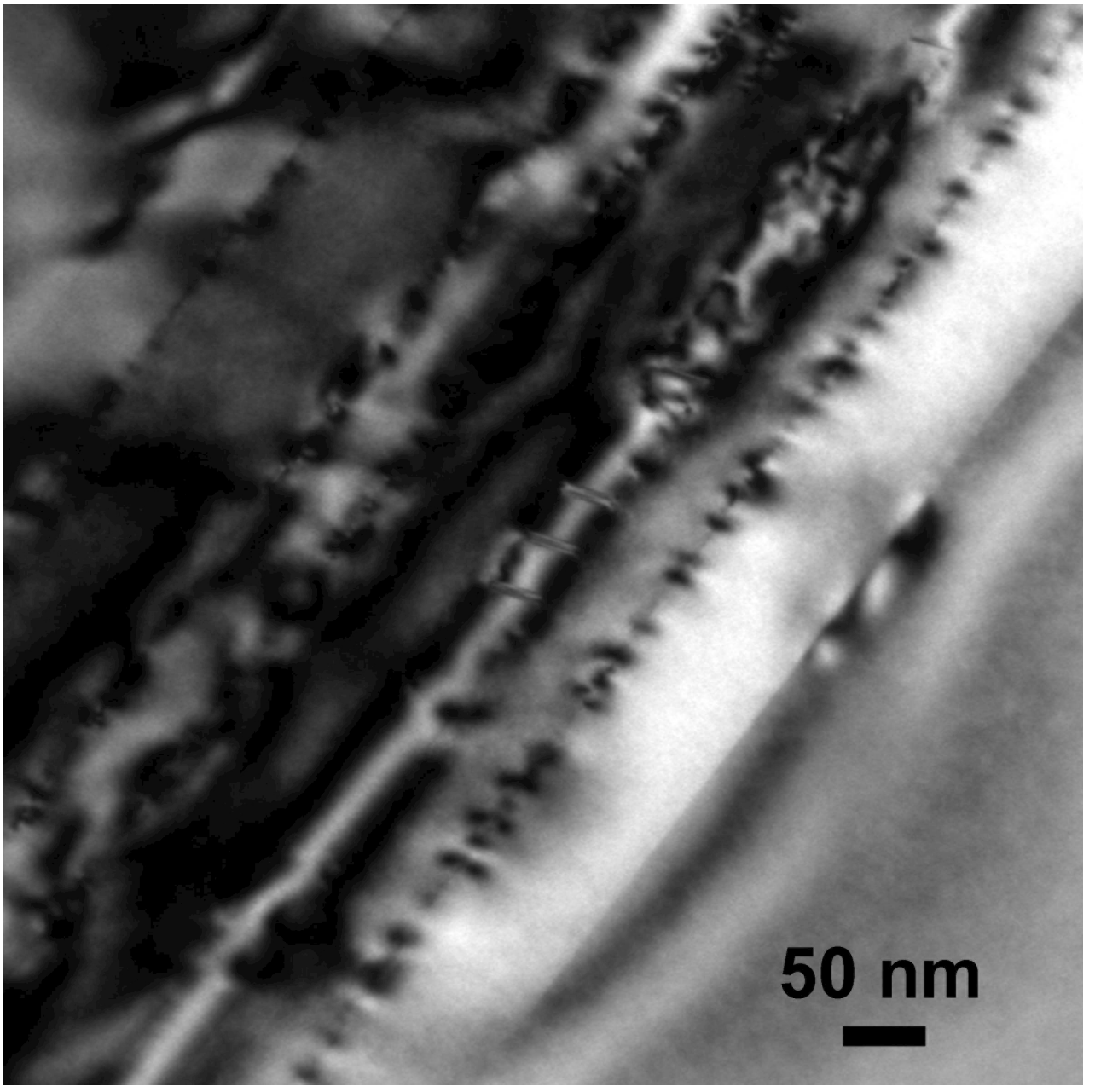
50 nm

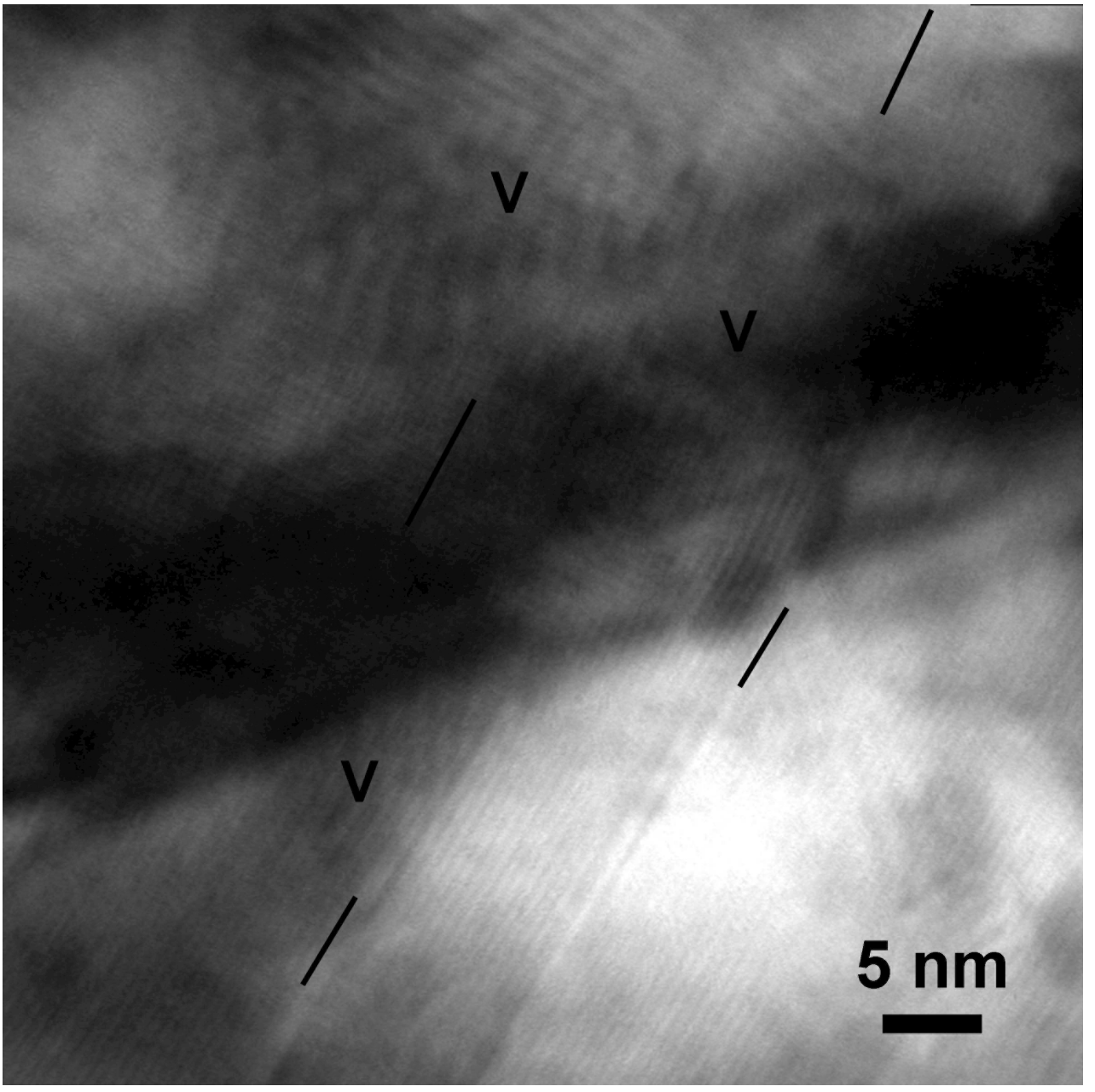
V
V
V
5 nm

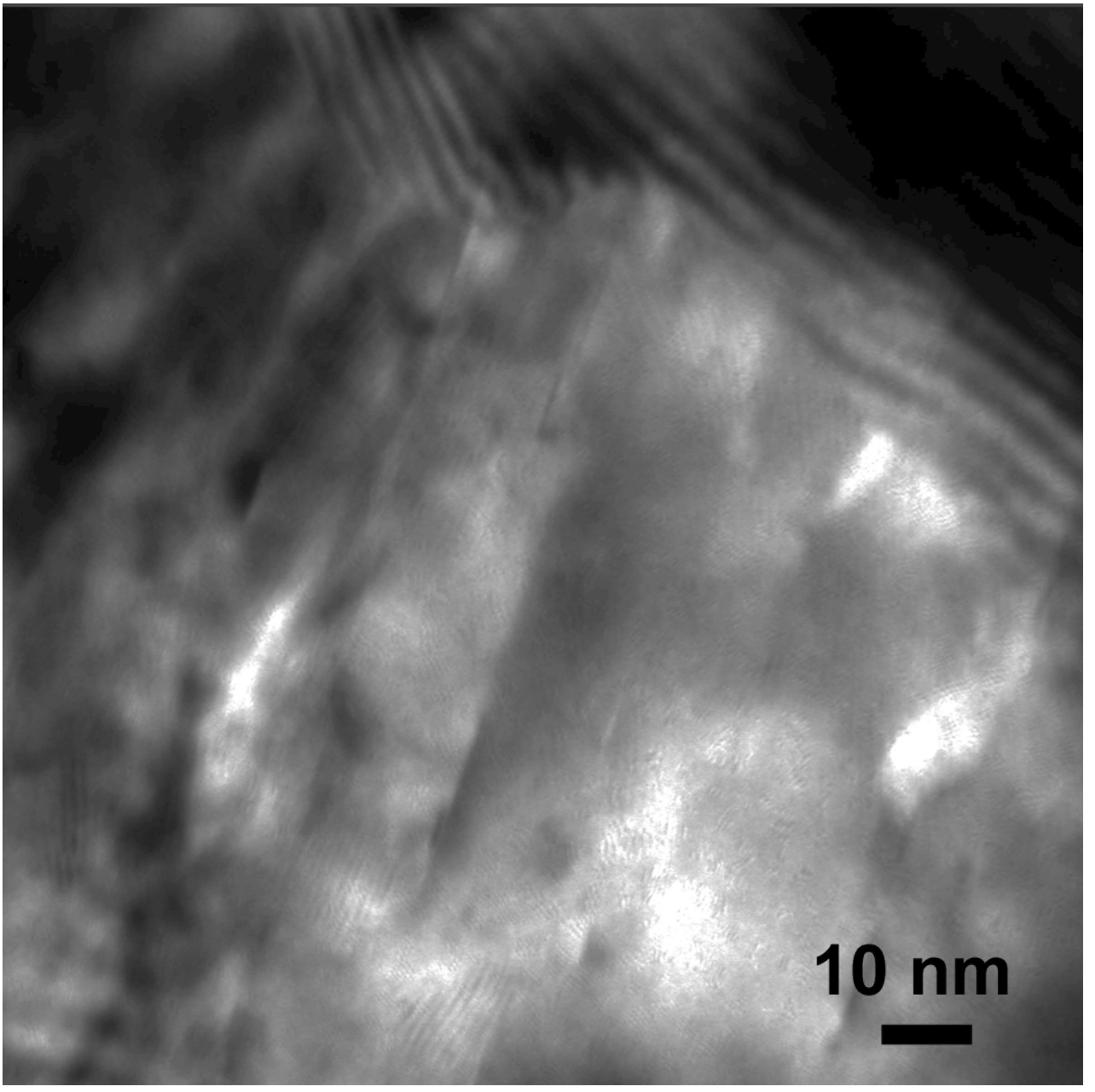
10 nm

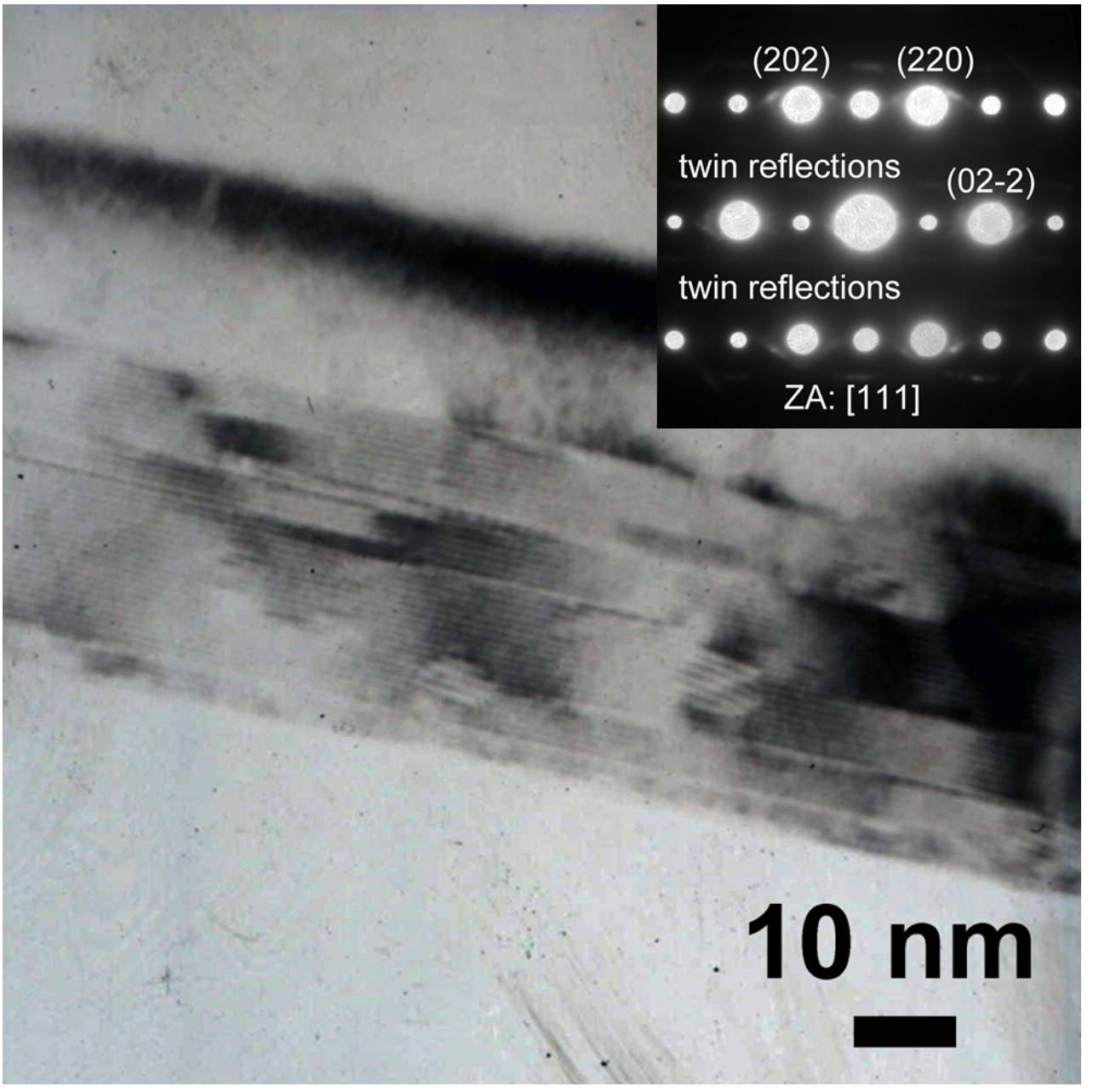
(202)
(220)
twin reflections
(02-2)
twin reflections
ZA: [111]
10 nm

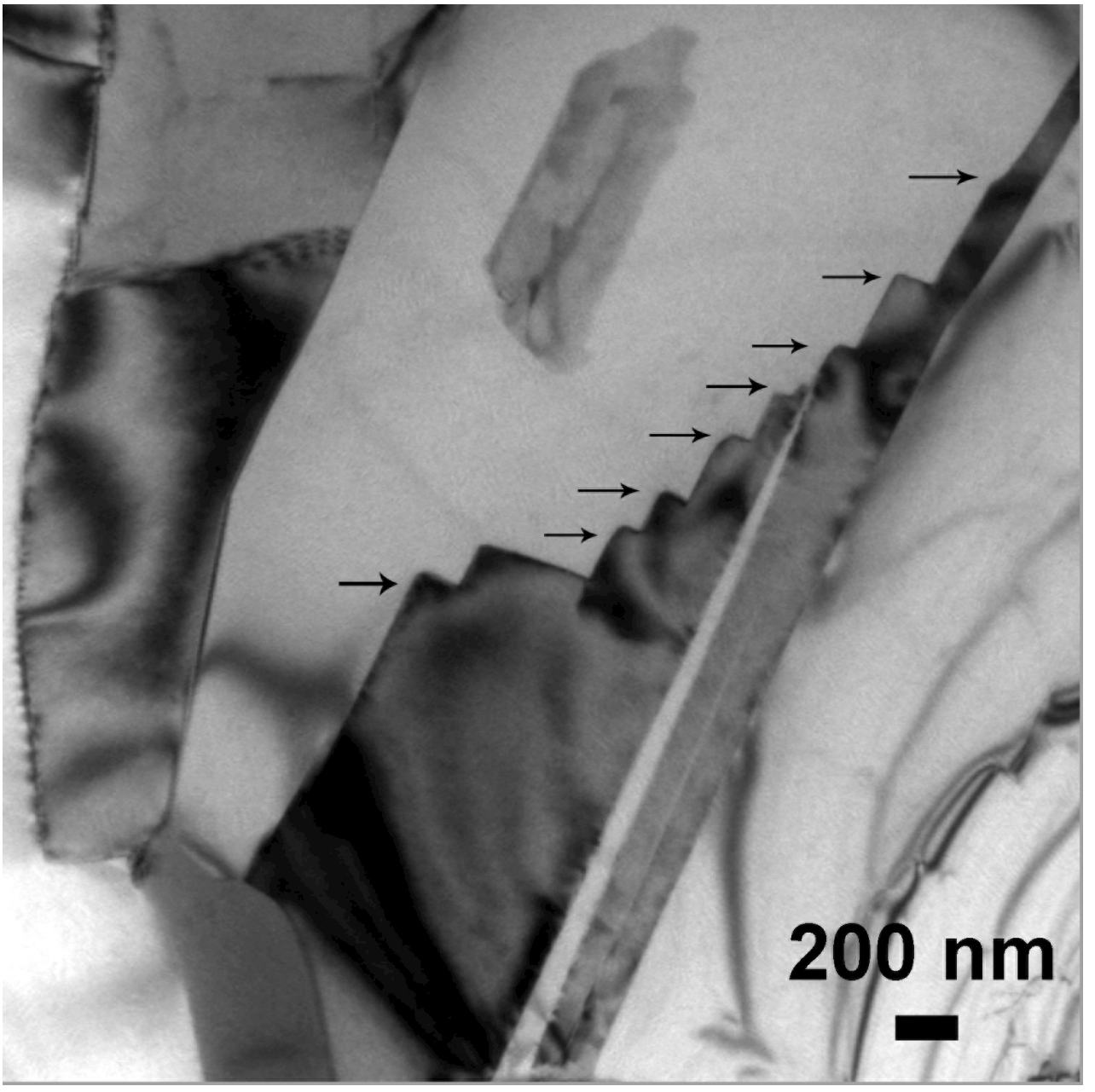
200 nm

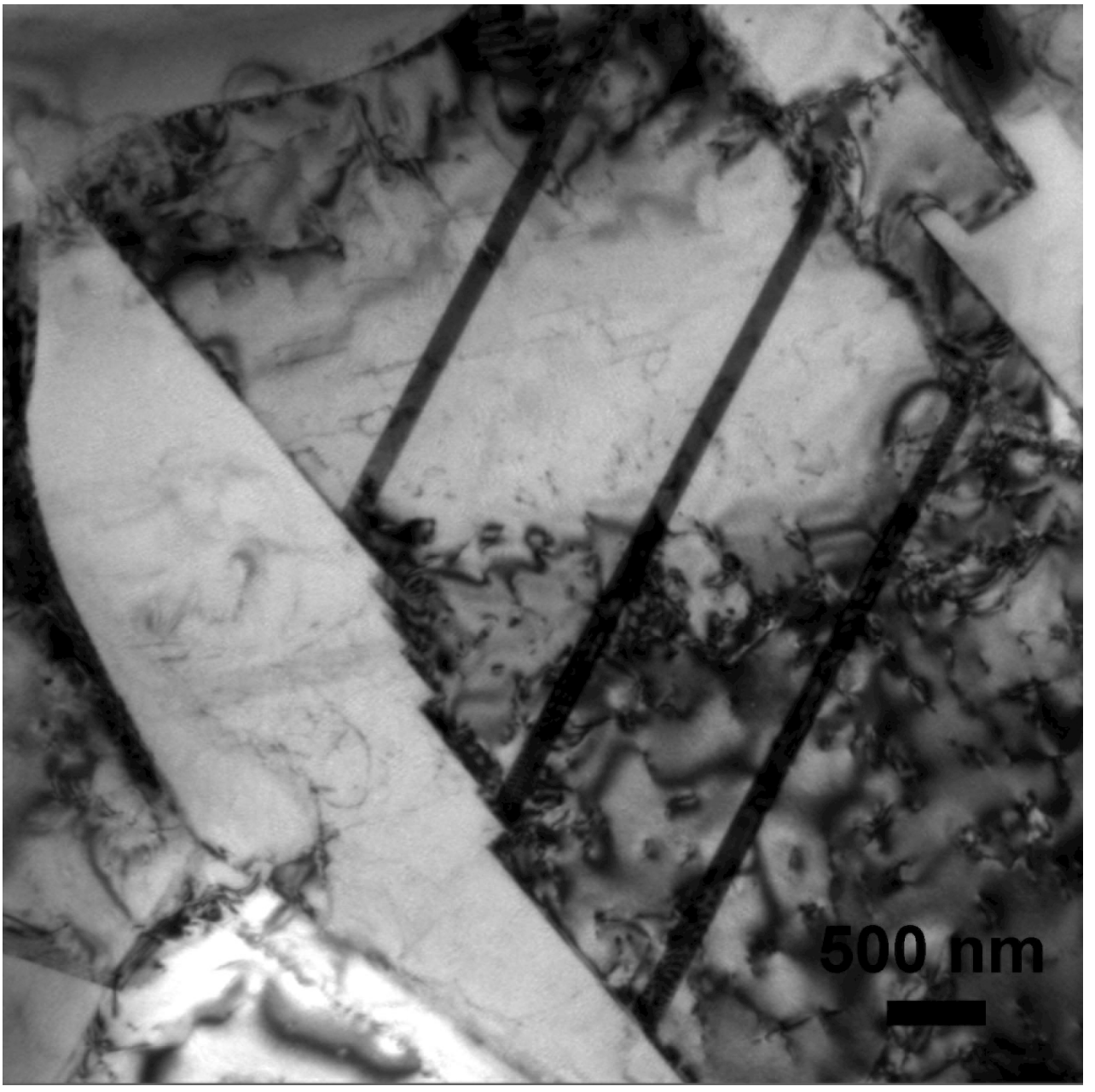
500 nm

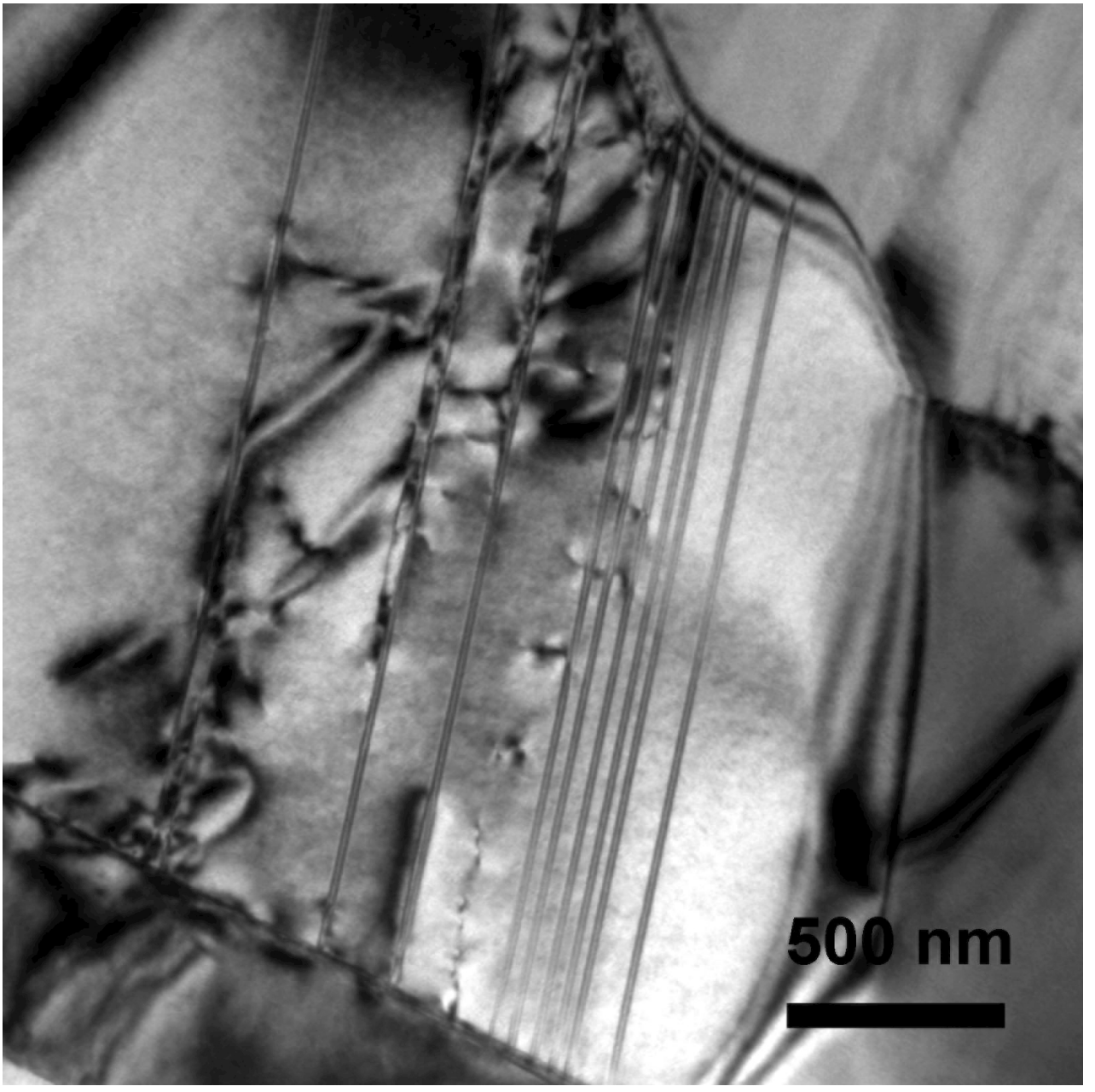
500 nm

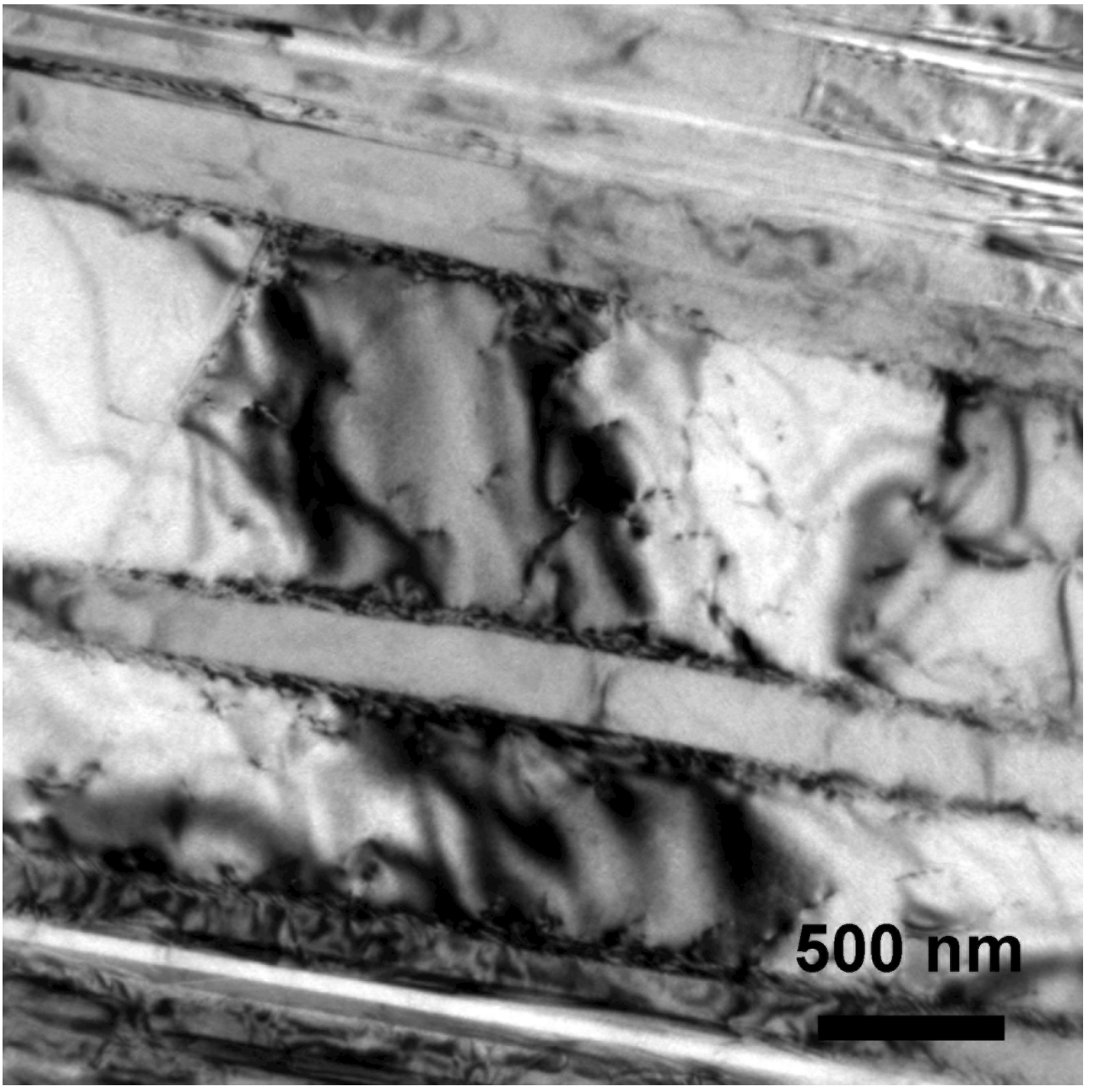
500 nm

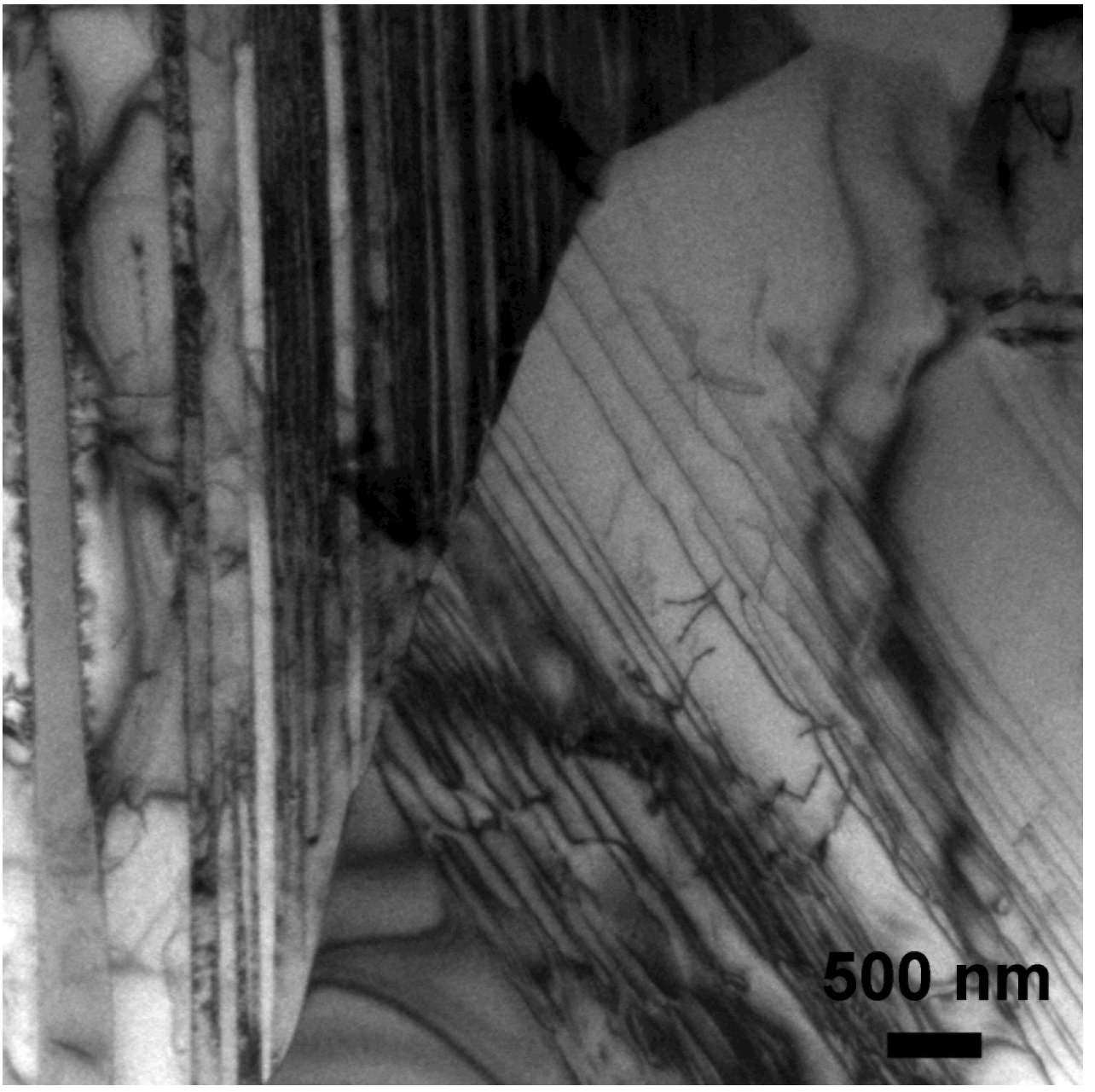
500 nm

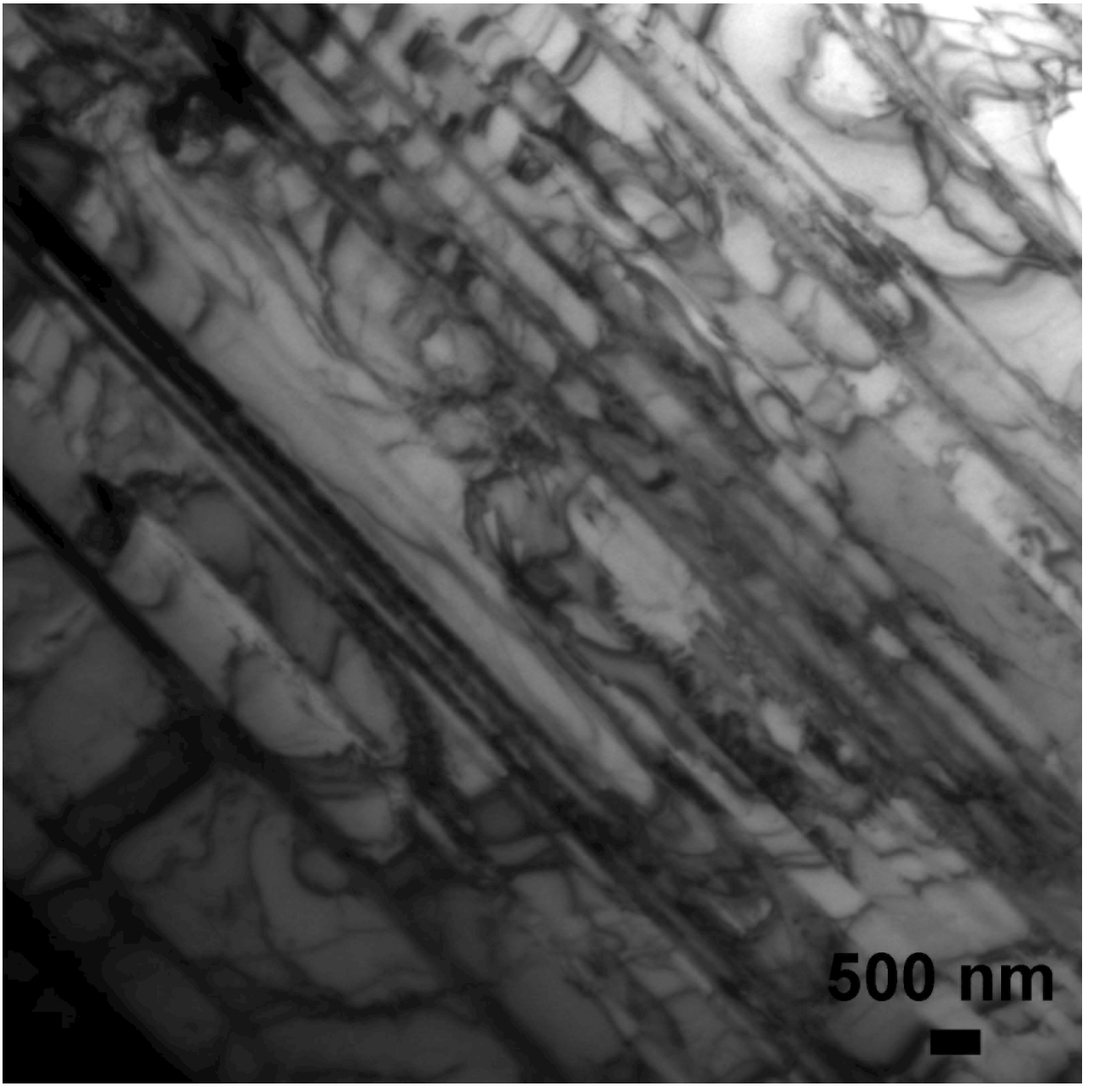
500 nm

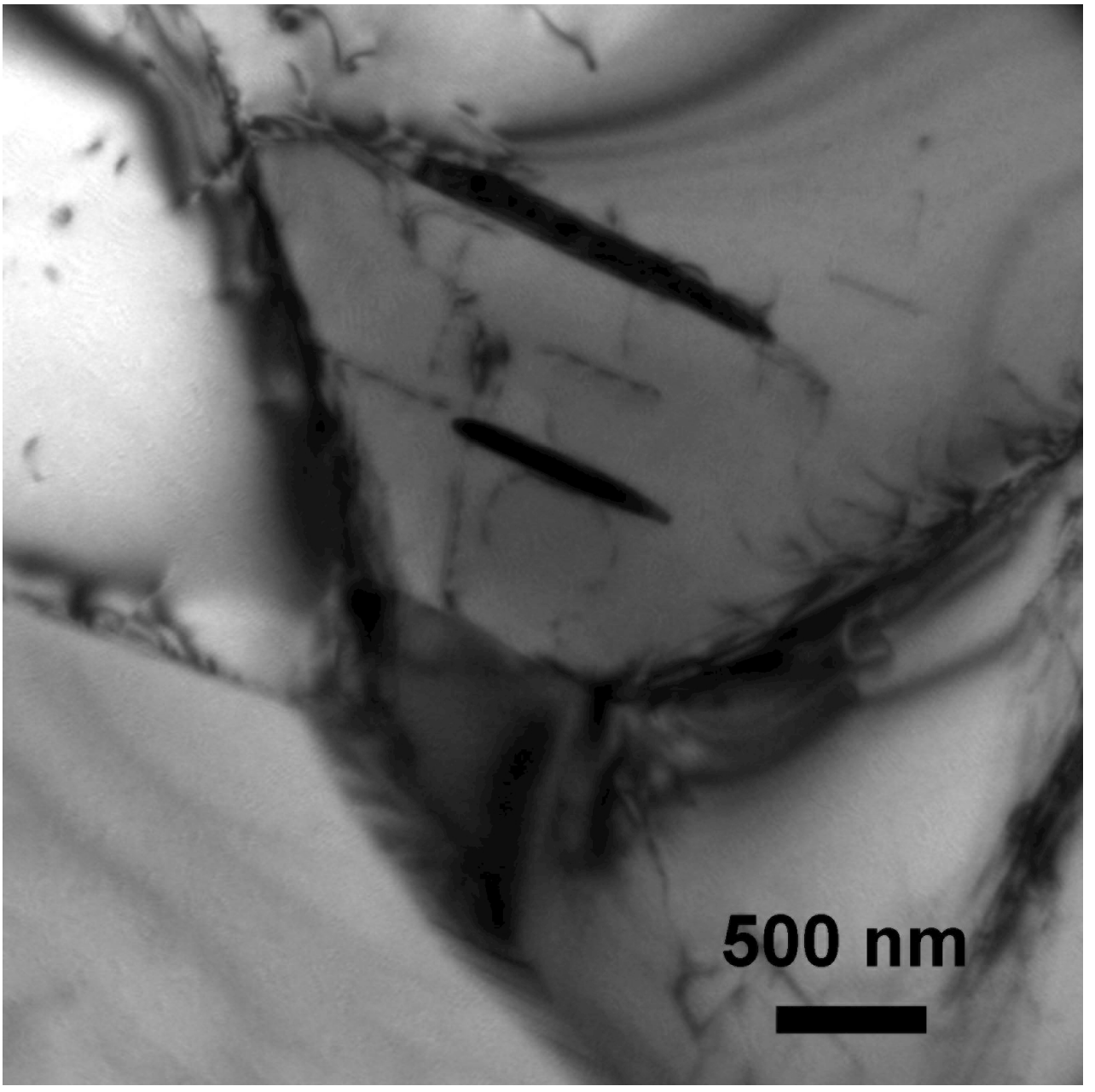
500 nm

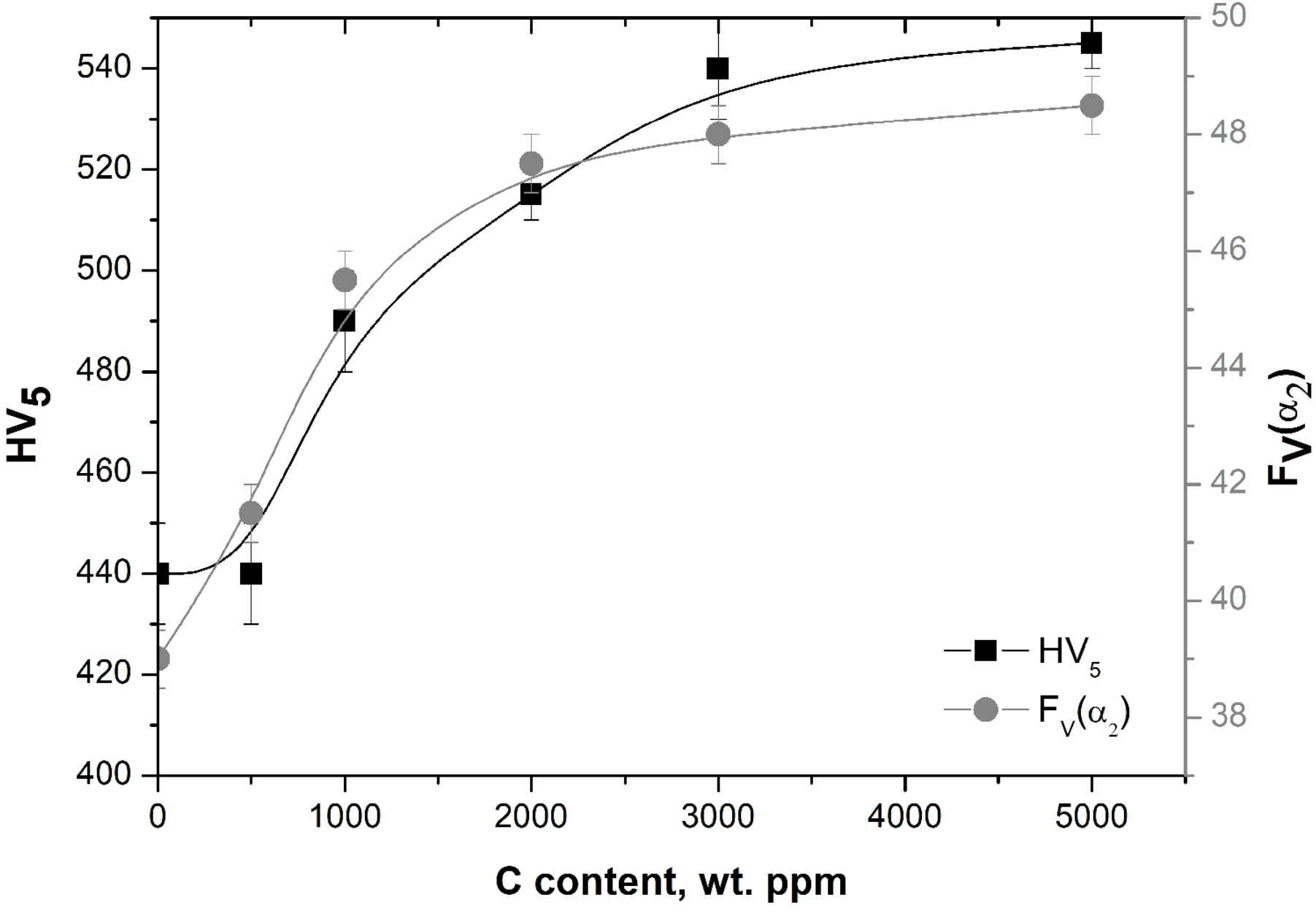
HV5
FV(α2)
C content, wt. ppm
HV5
FV(α2)
400
420
440
460
480
500
520
540
38
40
42
44
46
48
50
0
1000
2000
3000
4000
5000

Conflict of Interest statement

The manuscript is original and no part of it has been published before, nor is any part of it under consideration for publication at another journal. The author also declares no conflicts of interest.

Yours, sincerely,
Prof. Marcello Cabibbo

Author Statement
Man number Intermetallics_2019_1018

Dear Editor,
the author of this manuscript has replied to all the comments and remarks made by the three Reviewers. These were appended to the “Response letter” and all the needed changes were highlighted in yellow in the revised manuscript.

Yours,
Sincerely
Prof. Marcello Cabibbo

Data in brief

The role of carbon addition and aging temperature on the evolution of γ/γ and γ/α_2 interfaces in a dual-phase ternary Ti–46Al–4Nb intermetallic alloy was characterized by electron microscopy techniques. The study was extended to the alloy hardness modifiaction induced by the carbon addition to the alloy. In particular, the role of γ twins and α_2 lamellae widths on the hardness variation with carbon content was recognised and described.

H-Ti_2AlC phase formed at C > 3000 wt. ppm, anyhow the formation of *H*-Ti_2AlC phase did not change significantly the lamellar spacing.

Carbon in solid solution increased the α_2 volume fraction and decreased the mean distance between α_2 lamellae upon aging at 1273K.

By increasing carbon content the almost equal number fraction of variant-twinning, pseudo-twinning, perfect-twin and α_2 lath boundaries progressive changed in fsvour of a larger fraction of both perfect-twin and α_2 lath boundaries at the expense of the other two types of twin boundaries, variant-twin and pseudo-twin. The formation of the *H*-phase did not constrast this tendency, although it seemed to induce a process saturation.

Ti-46Al-4Nb microhardness was promoted to rise by the solute carbon content in the alloy up to a saturation limit at C ≅ 3000 wt. ppm, that is as soon as the *H*-phase started to form at the expense of the solute concentration. Corresppndingly, the α_2 lath volume fraction followed a similar trend with carbon content and it also saturated whenever carbon reached the alloy solute limit concentration to inititate the precipitation of the *H*-phase. Thence, the alloy hardness strongly depended on the α_2 lamellae width and volume fraction.